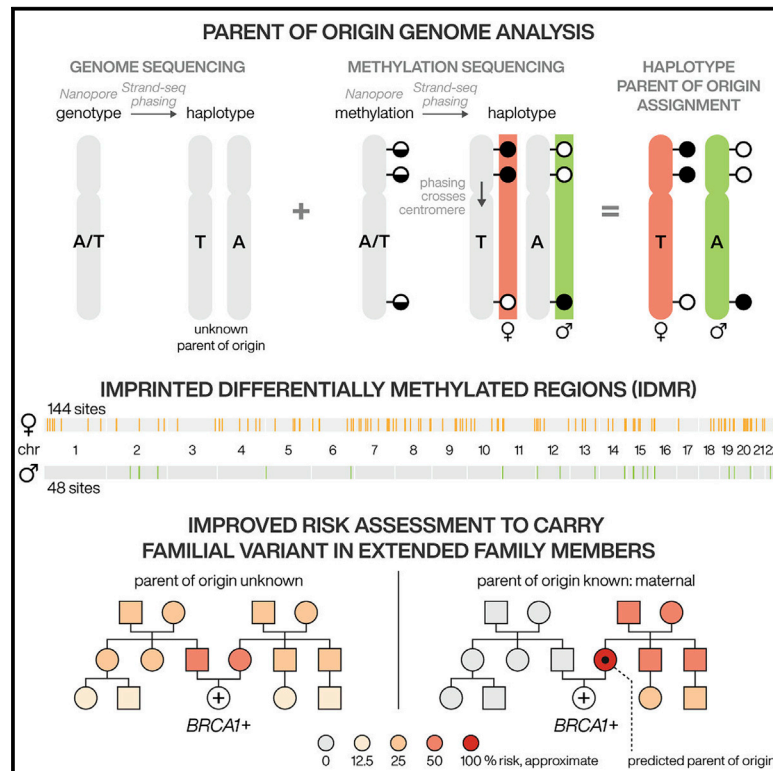


Parent-of-origin detection and chromosome-scale haplotyping using long-read DNA methylation sequencing and Strand-seq

Graphical abstract



Authors

Vahid Akbari, Vincent C.T. Hanlon, Kieran O'Neill, Louis Lefebvre, Kasmintan A. Schrader, Peter M. Lansdorp, Steven J.M. Jones

Correspondence

plansdor@bccrc.ca (P.M.L.), sjones@bcgsc.ca (S.J.M.J.)

In brief

Akbari et al. present a method for identifying homologous chromosomes inherited from the mother or the father without using data from the parents. The method relies on phased DNA methylation at maternally and paternally imprinted loci, as well as chromosome-length phasing of DNA sequence. Testing on five trios showed that the method can correctly infer the parent of origin of all autosomes with a mismatch error rate of 0.31% for SNVs.

Highlights

- Genomic imprinting can help infer the parent of origin of homologs
- Imprinted DNA methylation must be combined with chromosome-length haplotypes
- The method was validated for five trios with diverse genetic backgrounds
- In future, parent-of-origin phasing will improve cascade genetic testing



Short article

Parent-of-origin detection and chromosome-scale haplotyping using long-read DNA methylation sequencing and Strand-seq

Vahid Akbari,^{1,2,5} Vincent C.T. Hanlon,^{3,5} Kieran O'Neill,¹ Louis Lefebvre,² Kasmintan A. Schrader,^{2,4} Peter M. Lansdorp,^{2,3,*} and Steven J.M. Jones^{1,2,6,*}

¹Canada's Michael Smith Genome Sciences Centre, BC Cancer, Vancouver, BC, Canada

²Department of Medical Genetics, Faculty of Medicine, University of British Columbia, Vancouver, BC, Canada

³Terry Fox Laboratory, BC Cancer, Vancouver, BC, Canada

⁴Department of Molecular Oncology, BC Cancer, Vancouver, BC, Canada

⁵These authors contributed equally

⁶Lead contact

*Correspondence: plansdorp@bccrc.ca (P.M.L.), sjones@bcgsc.ca (S.J.M.J.)

<https://doi.org/10.1016/j.xgen.2022.100233>

SUMMARY

Hundreds of loci in human genomes have alleles that are methylated differentially according to their parent of origin. These imprinted loci generally show little variation across tissues, individuals, and populations. We show that such loci can be used to distinguish the maternal and paternal homologs for all human autosomes without the need for the parental DNA. We integrate methylation-detecting nanopore sequencing with the long-range phase information in Strand-seq data to determine the parent of origin of chromosome-length haplotypes for both DNA sequence and DNA methylation in five trios with diverse genetic backgrounds. The parent of origin was correctly inferred for all autosomes with an average mismatch error rate of 0.31% for SNVs and 1.89% for insertions or deletions (indels). Because our method can determine whether an inherited disease allele originated from the mother or the father, we predict that it will improve the diagnosis and management of many genetic diseases.

INTRODUCTION

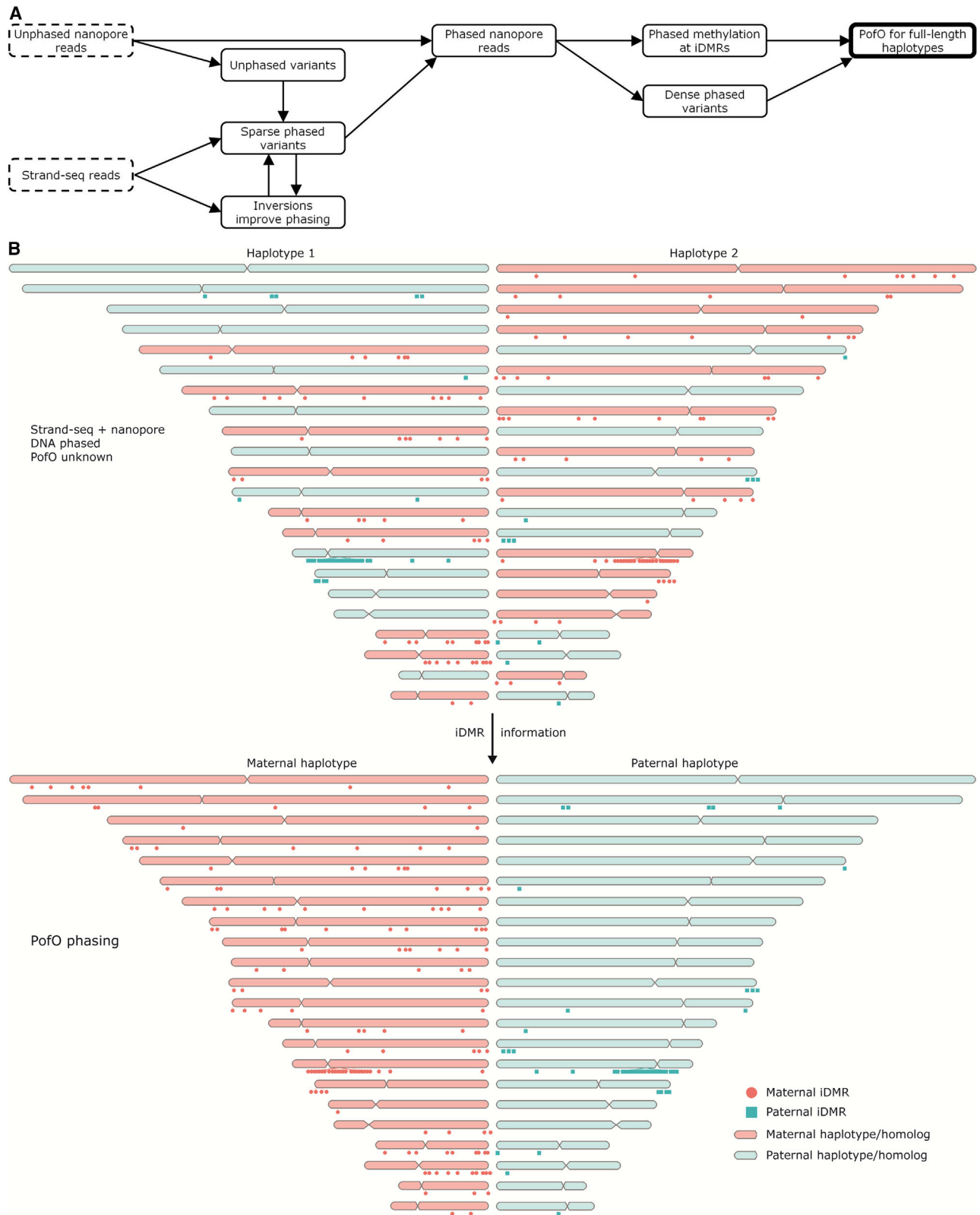
Although phasing is conventionally defined as the task of distinguishing alleles from maternal and paternal homologs, in practice most current phasing methods neglect parental information entirely. Instead, they group alleles from each chromosome or subchromosomal phase block into two haplotypes (for diploids), which correspond to different homologous chromosomes but are not assigned a parent of origin (PofO). These haplotypes can only be assigned a PofO if trio information of some kind is available, for example by comparing previously discovered alleles for the mother or the father with the child's alleles at heterozygous loci. In this sense, true phase information is largely out of reach for current genomic methods that do not incorporate sequence data from at least one parent next to the child.^{1–4}

A striking exception to this paradigm is the parental information provided by consistent differences in DNA methylation between maternally and paternally inherited alleles at imprinted differentially methylated regions (iDMRs). This differential methylation is either established in gametes and escapes the epigenetic reprogramming that follows fertilization or it is established after fertilization,^{5,6} and it persists through adulthood. iDMRs reliably suppress the expression of either maternal or paternal alleles at nearby genes or gene clusters and, crucially, can be detected in cell lines or fresh samples using the unique

ion current signature of 5-methyl-cytosine by nanopore sequencing (Oxford Nanopore Technologies).^{7–10} Long nanopore reads can be used to call both sequence variation and DNA methylation to detect genome-wide allele-specific methylation.^{9,10} Despite the fact that phasing using nanopore reads can achieve megabase-scale phase blocks, full chromosome haplotypes cannot be obtained, and each chromosome is represented in several phase blocks with likely switches between the paternal and maternal origin of the blocks along the chromosome.⁹

Conversely, some phasing techniques lack parental information but produce phase blocks that span centromeres, repetitive regions, and runs of homozygosity.^{11,12} Single-cell template strand sequencing (Strand-seq) is a library preparation method that captures parental DNA template strands in daughter cells cultured for one DNA replication round in the presence of BrdU.¹³ Reads from Watson template strands map to the reference genome in the minus orientation and reads from Crick template strands map in the plus orientation, meaning that alleles covered by reads with different orientations belong to different homologs. This approach enables the construction of global, chromosome-length haplotypes.¹¹ Because Strand-seq phase blocks are generally sparse (i.e., they do not phase all single-nucleotide variants [SNVs]), Strand-seq often serves as a scaffold upon which reads or subchromosomal phase blocks from





(legend on next page)

other sequencing techniques are combined, effectively phasing them relative to each other.^{14–17}

Determining a PofO for germline variants can aid in clinical genetics through variant curation, the efficient screening of relatives for genetic disease, and is essential to evaluate disease risk when a pathogenic variant has PofO effects, that is, when a patient's risk of disease depends on from which parent it is inherited (e.g., hereditary paraganglioma-pheochromocytoma syndrome due to pathogenic variants in *SDHD* or *SDHAF2*).^{18–22} Cascade genetic testing is used for pathogenic variants associated with diseases such as hereditary cancers with the goal of preventing or catching cancers early in family members.²³ In the absence of PofO information due to parents being unavailable, deceased, or declining genetic testing, cascade genetic testing must be offered to both sides of the family until segregation is confirmed. This may be costly and burdensome to patients and families, exacerbating already low rates of uptake of cascade genetic testing.^{24,25} Eliminating the need to test one side of the family is a clear benefit and a major clinical utility of defining a PofO for pathogenic variants, and more broadly, establishing chromosome-length haplotypes with accurate parental segregation of genomic variation has widespread applications.

We report that alleles along the full length of each human autosome can be assigned to the maternal or paternal homolog when nanopore methylation and iDMRs are integrated with Strand-seq chromosome-length haplotypes (Figure 1). This method does not require parental sequence data (trio information) or SNV linkage analysis but instead relies on the fact that all human autosomes have at least one iDMR of known parental origin. The only input required is a sample of fresh whole blood or other viable cells that can be cultured. We validated PofO assignment for heterozygous SNVs and insertions or deletions (indels) against five gold-standard trios from the Genome in a Bottle Consortium (GIAB), the Human Genome Structural Variation Consortium (HGSVC), and the 1000 Genomes Project (1KGP).^{16,26,27} By tracing pathogenic variants through families with sequencing efforts directed toward select family members, our method has the potential to transform cascade genetic testing and improve screening for genetic disease.

RESULTS

Nanopore and Strand-seq enable chromosome-scale haplotyping

We used five human genomes to demonstrate our approach, including NA12878; HG002 and HG005 from GIAB; HG00733 from HGSVC; and NA19240 from 1KGP.^{16,26,27} For all the samples, we used nanopore sequencing data at 24–38× depth of

coverage (Figure S1) and 42–220 Strand-seq libraries with 2.78–9.46× combined depth of coverage per sample (Figure S2). Nanopore raw signals were base called and mapped to the human reference genome GRCh38. SNVs and indels (“variants”) were called from nanopore reads using Clair3²⁸ (Figure S3). The SNV callsets for each individual included nearly all SNVs in the five corresponding ground truth callsets (mean [M]: 97.98%, standard deviation [SD]: 1.67%, range: 95.51%–99.64%; Table 1), while fewer indels were recovered (M: 64.01%, SD: 8.43%, range: 52.69%–78.18%). For both SNVs and indels, we recovered the greatest proportion of ground-truth variants in the individual with the greatest nanopore coverage, while we recovered the smallest proportion in the individual with the least coverage. This suggests that including more nanopore data would be one way to address the high false-negative rate for indels.

Before iDMRs can be used to assign a PofO to homologs, chromosome-length haplotypes must be constructed. This is because iDMRs cover only a small fraction of the autosomal human genome (estimated in this study to be 0.014%) and are not necessarily phased relative to variants. While nanopore reads alone can be used to phase nearly all called variants for each sample, the resulting phase blocks are relatively short ($N50\ M \pm SD = 4.85 \pm 3.66$ Mb), do not span full chromosomes, and do not all contain iDMRs (Figures S4 and S5). We therefore applied inversion-aware Strand-seq phasing to the nanopore SNVs first and constructed sparse, chromosome-length haplotypes. Strand-seq phased 60.62–94.89% of the common heterozygous SNVs between the ground-truth and nanopore callsets with 0.14%–1.36% mismatch error rates (number of incorrectly phased variants/number of all phased variants), with each chromosome spanned by a single phase block (Tables 1, S1, and S2; Figures S4 and S6). Strand-seq-phased SNVs were then used to phase nanopore reads (fraction of reads with at least MAPQ 20 that were successfully phased, $M \pm SD: 71\% \pm 9.6\%$), which were, in turn, used to re-phase all variants and achieve dense, chromosome-scale haplotypes containing nearly all heterozygous SNVs and most indels (Tables 1 and S1). Combining Strand-seq and nanopore in this way allowed us to phase 99.39%–99.91% of the heterozygous SNVs and 96.41%–98.77% of the heterozygous indels that were present in both the ground-truth and nanopore callsets, with mismatch error rates 0.07%–0.54% for SNVs and 1.33%–2.43% for indels (Tables 1 and S1). Our phasing approach used the GRCh38 reference genome, and we did not perform *de novo* genome assembly of any kind.

iDMRs assign PofO to haplotypes

PofO-specific DNA methylation at iDMRs provides a unique source of information to determine the PofO of homologs,

Figure 1. Overview of the parent-of-origin (PofO) phasing method

(A) The inputs for the workflow are nanopore long reads and data from single-cell Strand-seq libraries. Nanopore data are used to call variants, some of which are phased with Strand-seq in an inversion-aware manner. These phased variants are then used to phase the nanopore reads, which are used to phase more variants and DNA methylation. Finally, the DNA methylation status of iDMRs is used to identify the PofO for each homologous chromosome.

(B) Without examining DNA methylation, Strand-seq and nanopore reads can be combined to construct chromosome-length haplotypes,^{14,16} but the assignment of each homolog (i.e., chromosome-length haplotype) to haplotype 1 or haplotype 2 (HP1 or HP2) is random with respect to its PofO, as shown by this cartoon. However, iDMRs can be used to distinguish maternal and paternal homologs. Lollipops mark the locations of all 144 maternal iDMRs used in this study (methylated on the maternal homolog) and all 48 paternal iDMRs.

For iDMR names and locations shown relative to cytobands, see Figure S7.

Table 1. Phasing of heterozygous variants and comparison with the ground-truth callset

Heterozygous SNVs	HG002	HG005	HG00733	NA12878	NA19240
Total in ground-truth callset	2,117,525	1,922,666	2,168,512	2,027,097	2,787,148
Common between nanopore and ground truth	2,100,326	1,915,821	2,071,156	2,009,263	2,688,200
Strand-seq switch rate	0.0202	0.0078	0.0087	0.002	0.0055
Strand-seq switch/flip rate	0.0112	0.0044	0.0049	0.0012	0.003
Strand-seq mismatch rate	0.0136	0.006	0.0067	0.0014	0.0048
Strand-seq number of correctly phased	1,496,173	1,516,727	1,255,486	1,906,619	1,903,540
Strand-seq number of incorrectly phased	20,560	9,155	8,457	2,730	9,239
Combined Strand-seq and nanopore switch rate	0.0016	0.0011	0.0027	0.0008	0.0029
Combined Strand-seq and nanopore switch/flip rate	0.001	0.0007	0.0016	0.0005	0.0016
Combined Strand-seq and nanopore mismatch rate	0.0054	0.0024	0.0034	0.0007	0.0035
Combined Strand-seq and nanopore number of correctly phased	2,076,204	1,903,642	2,061,700	2,001,412	2,676,235
Combined Strand-seq and nanopore number of incorrectly phased	11,256	4,634	7,017	1,489	9,414
Heterozygous indels	HG002	HG005	HG00733	NA12878	NA19240
Total in ground-truth callset	326,220	250,169	286,492	292,829	335,801
Common between nanopore and ground truth	215,614	195,590	150,941	186,625	199,359
Combined Strand-seq and nanopore switch rate	0.0409	0.0397	0.0237	0.0334	0.0323
Combined Strand-seq and nanopore switch/flip rate	0.0213	0.0206	0.0124	0.0172	0.0167
Combined Strand-seq and nanopore mismatch rate	0.0243	0.0218	0.0133	0.0174	0.0177
Combined Strand-seq and nanopore number of correctly phased	202,815	184,615	147,100	178,390	193,356
Combined Strand-seq and nanopore number of incorrectly phased	5,061	4,106	1,986	3,161	3,477

We include only biallelic heterozygous variants in the ground-truth callset (0/1, 1/0, 0|1, or 1|0) for consistency with the phasing error rate calculations. See also [Table S1](#).

represented by chromosome-length haplotypes, without using parental sequence data. We assembled a list of 192 iDMRs from previous genome-wide studies^{6,29–32} (see [STAR Methods](#); [Figure S7](#); [Table S3](#)). Chromosome X was ignored as it is not generally thought to have iDMRs. We combined DNA methylation information from phased nanopore reads with the known PofO information at the imprinted intervals to assign the PofO to each homolog (see [STAR Methods](#)). On average, 5.7 iDMRs (median: 5, SD: 5.2, range: 1–29) were used for PofO assignment of each chromosome, and each chromosome was assigned to its parental origin with an average of 95.7% confidence score (median: 99%, SD: 7.2%, range: 57.5%–100%; see [STAR Methods](#); [Figures 2](#) and [S8–S11](#); [Table S4](#)). On average, 7% of

iDMRs conflicted with the majority PofO assignment. However, because iDMRs are weighted by the degree of differential methylation in each sample, conflicting iDMRs represented only 3% of the PofO contribution values (x_i ; see [STAR Methods](#); [Table S4](#)).

We examined 220 autosomal homologs across five individuals in this study (5 individuals \times 22 autosomes \times 2 ploidy) and compared the inferred PofO with the trio-assigned PofO in the ground-truth-phased variant callsets. All 220 homologs were correctly assigned a PofO, that is, the chromosome-length haplotype was correctly identified as either maternal or paternal and had few phasing errors (chromosome-level mismatch error rates for SNVs, $M \pm SD$: 0.34% \pm 0.53%, range: 0.03%–4.86%; for

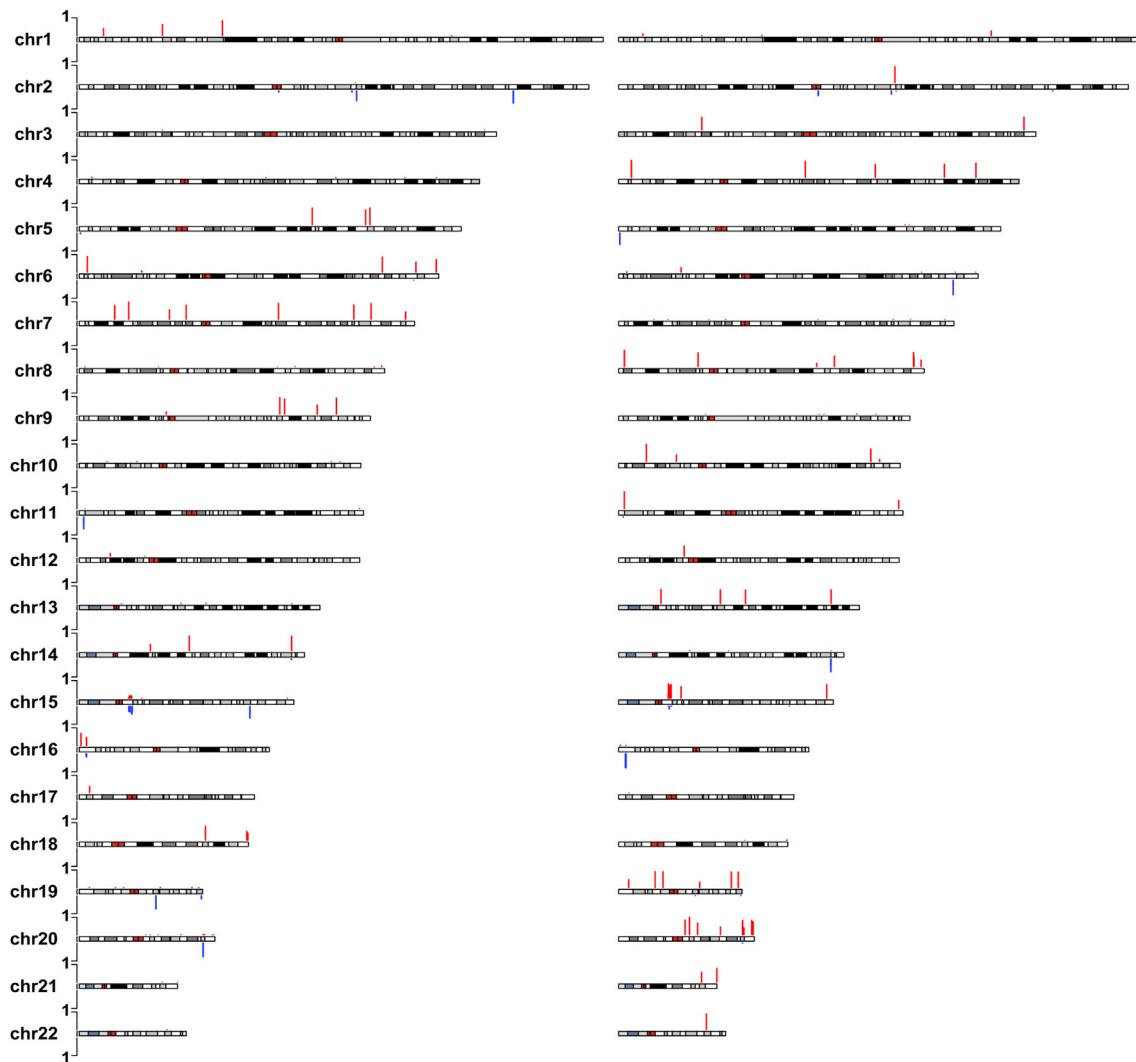


Figure 2. CpG methylation at paternal and maternal iDMRs used for PofO assignment in HG002

Maternally methylated iDMRs are red and upward and paternally methylated iDMRs are blue and downward. Bars represent the fraction of CpGs with methylation differences ≥ 0.35 (differential methylation) between haplotypes (HP1 – HP2 for haplotype 1, which is on the left side, and HP2 – HP1 for haplotype 2, which is on the right side) at each iDMR for each haplotype. The chromosomes themselves are colored according to Giemsa banding (white, gray, and black), with the centromeres in red and the stalks of acrocentric chromosomes in blue-gray. See also [Figures S8–S11](#).

indels, $M \pm SD$: $1.93\% \pm 0.58\%$, range: 0.98%–5.35%; [Figures 3](#) and [S12](#); [Table S1](#)).

Roughly half of the iDMRs used were reported in at least two previous studies, while the rest were reported in just one study and confirmed by partial methylation observed among 179 WGBS datasets from 119 blood and 60 tissue samples (see [STAR Methods](#)). One potential weakness of the single-study iDMRs is that 38 of them (19.8%) come from a previous study of 12 trios that included the same five trios examined here,³² and it is possible that some of these iDMRs might provide misleading or insufficient PofO information when examined in new individuals (i.e., if they are not truly imprinted). We tested the dependence of PofO phasing on the single-study iDMRs by re-running PofO assignment using only the 93 iDMRs found

in at least two studies: 208 of 220 autosomal homologs were correctly assigned a PofO (94.5%), while chromosome 5 was not assigned a PofO for NA19240 and chromosome 12 was not assigned a PofO for any individual because it did not have an iDMR. This suggests that PofO phasing is not reliant on poorly characterized iDMRs, likely because all autosomes have at least three iDMRs (in the full set of 192), with the exception of chromosome 17, which has one, and chromosome 3, which has two. This redundancy helps maintain robust PofO assignment even when some putative iDMRs provide weak or conflicting parental information. At a few iDMRs in some samples, for example at *TRPC3* on chromosome 4 in NA12878, we detected slight hypermethylation on the parental allele that is reported to be unmethylated: this might be due to inaccuracies in methylation calling or

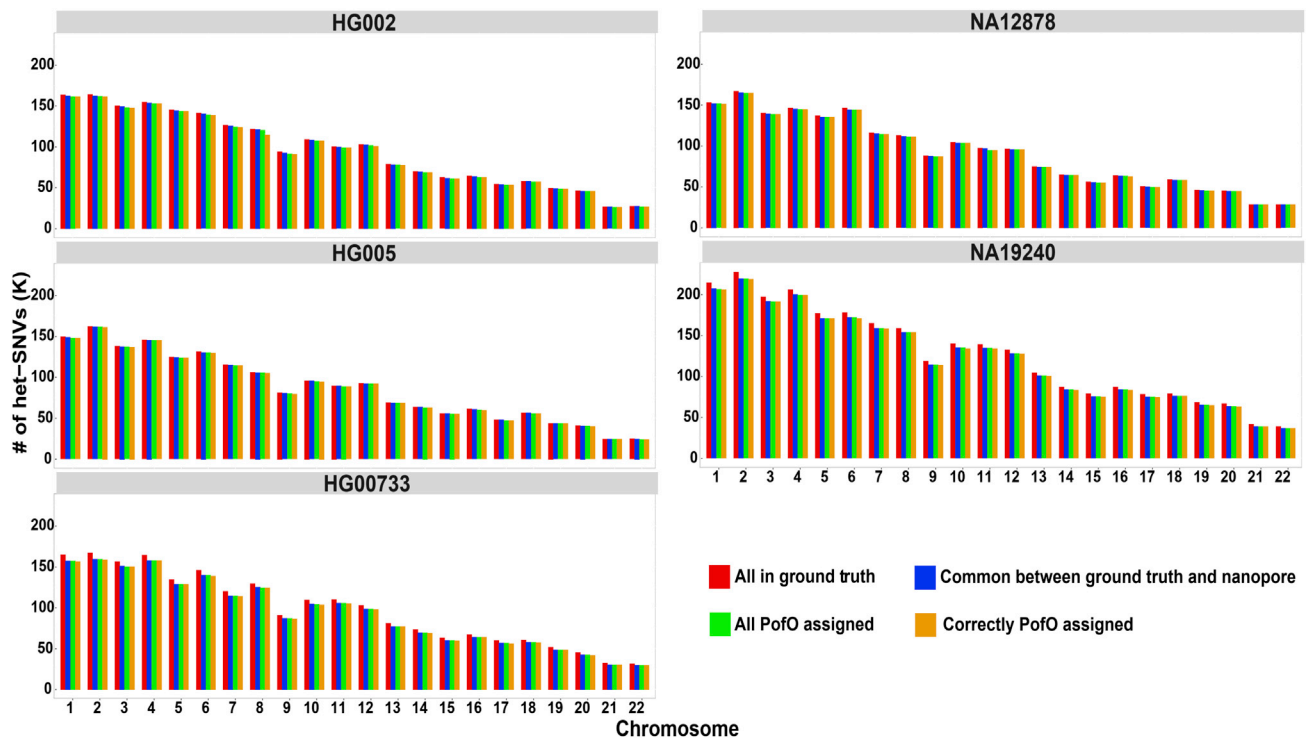


Figure 3. Per-chromosome results for PofO assignment of heterozygous (het)-SNVs

PofO could be assigned to all homologs. The small fraction of variants with incorrect PofO are sporadic phasing errors in the Strand-seq or nanopore data or local clusters of phasing errors on chromosomes 8 and 9, in the case of HG002.

See also [Figure S12](#).

phasing of nanopore reads, or it could reflect random allelic methylation rather than imprinting. Such methylation discrepancies could conceivably assign the wrong PofO to homologs. In this instance, additional iDMRs on the same chromosome enabled correct PofO assignment, albeit with the lowest confidence score (57.5%).

For additional confirmation that PofO phasing extracts reliable parental information, we calculated Mendelian error rates between each child's inferred parental haplotypes and ground-truth variant genotypes for their parents ([Figures 4](#) and [S13–S16](#); see [STAR Methods](#)). Local phasing errors are indicated by elevated Mendelian error rates at a large common inversion on chromosome 8 for HG002 (mismatch rate 99.86% for SNVs and 97.05% for indels inside the inversion at chr8: 8120810–12362538), which is the individual with the most phasing errors overall (SNV mismatch rate 0.54%; [Table 1](#)), as well as at the centromere for chromosome 9. The latter is in fact a single bin of 1,000 SNVs stretched across the centromere, which exaggerates its importance in [Figure S13](#). Globally, Mendelian error rates for maternal-mother and paternal-father comparisons were low ($M \pm SD$: $0.27\% \pm 2.69\%$; calculated for non-overlapping bins of 1,000 variants), while they were high for maternal-father and paternal-mother comparisons (representing misassigned PofO; $M \pm SD$: $25.75\% \pm 14.14\%$). For maternal-mother and paternal-father comparisons, the highest mean error rate for any chromosome was 2.29% for chromosome 8 in HG002. This is less than one-eighth of the lowest mean error rate for

any chromosome in maternal-father and paternal-mother comparisons (19.69% for chromosome 21 in NA12878), suggesting that the PofO assignment is correct for all chromosomes.

DISCUSSION

We show that homologous chromosomes, represented by chromosome-length haplotypes of SNVs and indels, can be assigned a PofO without using parental sequence data. Long nanopore reads provide DNA sequence information along with PofO information in the form of DNA methylation differences between maternal and paternal alleles at known iDMRs. Strand-seq libraries provide sparse global haplotype information that phases variants and nanopore reads to reconstruct individual homologs. The PofO of each homolog can then be determined based on the consensus of one or more embedded iDMRs ([Figure 1](#)).

PofO phasing has the potential to address immediate clinical needs in the diagnosis and management of genetic disease. These include improving variant curation and estimates of disease penetrance through co-segregation of variants to each side of the family with and without relevant disease phenotypes, determining which parent may have a risk for mosaicism in the context of a *de novo* variant, and establishing appropriate screening recommendations for pathogenic variants in genes with known PofO effects—as seen with *SDHD* and *SDHAF2*.^{18–22} Furthermore, PofO phasing provides a considerable advantage over current clinical testing in facilitating cascade genetic testing

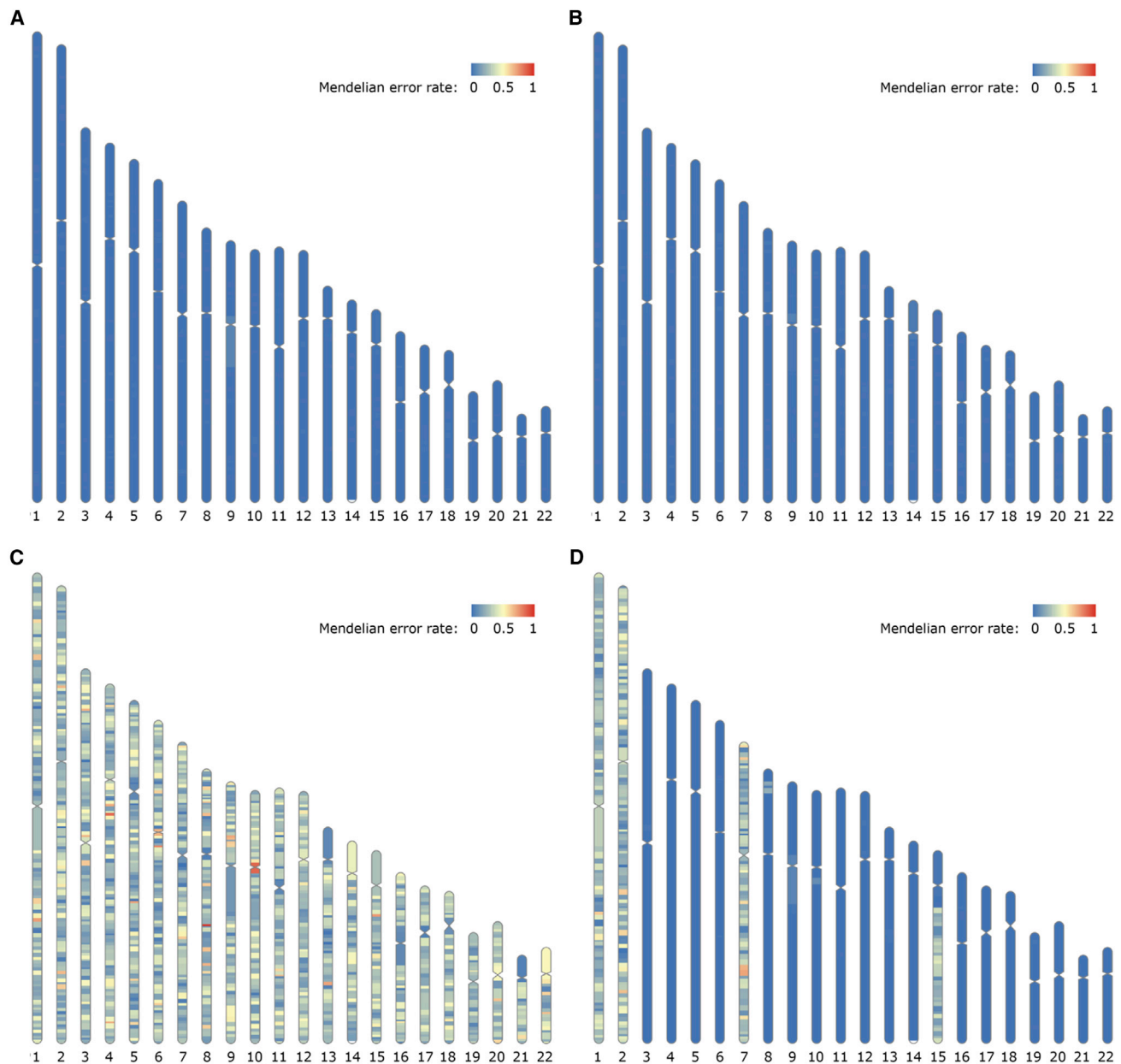


Figure 4. Mendelian error rates show that PofO phasing correctly infers parental haplotypes

(A) The inferred maternal haplotype for HG005 (child) is compared with the ground-truth variant genotypes for HG007 (mother). The Mendelian error rate is low across all chromosomes.

(B) The inferred paternal haplotype for HG005 (child) is compared with the ground-truth variant genotypes for HG006 (father).

(C) The inferred maternal haplotype for HG005 (child) is compared with the ground-truth variant genotypes for HG006 (father). This is the expected pattern if a PofO is misassigned for all chromosomes.

(D) We artificially produced chromosomes and regions with incorrect PofO assignments in the comparison of HG005's maternal haplotype with HG007. The lack of such regions is evidence that the PofO phasing method correctly distinguishes maternal and paternal homologs. We switched the maternal and paternal haplotypes for chromosomes 1, 2, and 7 to simulate erroneous iDMR inferences, and we created a large switch error on chromosome 15 by reducing the bin size in the BreakpointR step.³³

See also [Figures S13–S16](#).

that allows opportunities for intervention in actionable genetic diseases.³⁴ Contacting, counseling, and testing relatives is a significant logistical and financial burden to patients and healthcare systems, especially when considering adult-onset conditions,

where testing of parents is frequently not possible. Cascade genetic testing may be hindered by limited intrafamily communication and fractured family structures and has low uptake in ethnic minority populations.²⁵ PofO phasing stands to enable focused

approaches to cascade genetic testing throughout families, bringing goals of optimal cascade genetic testing rates within reach.³⁵ Of importance, the ability of PofO phasing to infer the pathogenic variant status of a patient's parent with a high degree of certainty is likely to place an even greater emphasis on the duty to warn at-risk individuals of actionable genomic findings that may have been primarily or secondarily sought throughout the course of genetic testing. Similar issues are already familiar to clinical genetics in the setting of obligate carriers, but because this approach need only test a single person to reconstruct the complete genomic contribution from each parent, there will be ethical considerations if PofO phasing is integrated into mainstream clinical genetic testing due to the unprecedented scale.

Other sequencing technologies could perhaps provide the DNA methylation, DNA sequence, and long-range phase information required for PofO phasing, or different methods could be used to combine them. For instance, PofO could be assigned to *de novo* trio-free diploid assemblies^{15,36} rather than chromosome-length haplotypes of small variants. SMRT sequencing (Pacific Biosciences), which now provides accurate DNA methylation as well as DNA sequence,³⁷ might be a substitute for nanopore data that provides better indel detection, and long-range phasing with Hi-C³⁶ could perhaps be used instead of Strand-seq, although if phase switches occur at centromeres,¹⁶ then chromosome arms that lack iDMRs (16q, 17q, 18p, and 20p) may not be assigned to a PofO.

Sequencing costs for PofO phasing are relatively low, with as little as 24× nanopore and 3× Strand-seq coverage used in this study. The DNA methylation information that underlies PofO assignment is robust and can easily be extracted from nanopore sequence data, while formerly rare Strand-seq libraries can now be produced in large numbers (>1,000) at a reduced cost.³⁸ In principle, genomic regions that are identical by descent in distant relatives could also be leveraged to partially assign PofOs with large SNV datasets, using either the sex chromosomes or the ethnicity of the parents, but such bioinformatic approaches would require that parents differ substantially in genetic background and would be subject to well-known ethnic biases in genomic datasets.³⁹ Given the simplicity and accuracy of PofO phasing, the lack of trio-free alternatives at present for extracting PofO information from genomic data, and the method's remarkable clinical applications, PofO phasing has the potential to become a routine component of genomic analysis.

Limitations of the study

In addition to the possibility that some putative iDMRs may not in fact be imprinted (see [results](#)), true iDMRs may display biological variability that could prevent PofO assignment for some chromosomes in new individuals or in other tissues or cell types that have fewer or different somatic iDMRs than the cell lines used in this study. Even though the paternal or maternal origin of methylation at iDMRs is consistent whenever just one allele is methylated, imprinted methylation can be variable in the sense that the two parental alleles may have similar amounts of DNA methylation in some tissues and individuals.^{6,40} In rare cases, epimutation or genomic imprinting disorders may also alter DNA methylation at iDMRs.⁴¹ Although redundant iDMRs (see [results](#)) should generally allow PofO assignment even in the

presence of such limited inter-individual and inter-tissue variability, ultimately, our method must be tested on additional trios from diverse genetic populations to determine which chromosomes are troublesome for PofO phasing. Advances in characterizing human DNA methylation may further improve PofO phasing by identifying additional iDMRs on iDMR-poor chromosomes (e.g., chromosome 17), by removing spurious iDMRs, and perhaps even by enabling PofO assignment for the X chromosome in females.⁴²

Even when a homolog is assigned the correct PofO overall, local phasing errors can cause incorrect PofO assignment for some variants. The chromosome-length haplotypes constructed in this study are highly accurate, however, with mean mismatch error rates of 0.31% for SNVs and 1.89% for indels. Although we identified only 64.01% of the indels in the ground-truth dataset, this reflects a limitation of current nanopore technology and would be straightforward to improve with the addition of short Illumina reads.^{28,43} We observed rare switch errors for SNVs and indels primarily at centromeres and at inversions (e.g., an inversion on chromosomes 8 in HG002 caused the largest mismatch error rates; [Figures 3](#) and [S13](#); [Table S1](#)), but these generally contain few variants. Phasing errors at centromeres are likely due to misaligned reads in repetitive sequences, while errors at inversions are due to changes in sequence orientation that disrupt the directional information Strand-seq exploits for phasing.¹¹ Inversion-related phasing errors can be partially addressed with a new StrandPhaseR function that re-phases variants inside known inversions.⁴⁴ This is essential when iDMRs fall inside inversions, where they may support the wrong PofO if phasing is not corrected (e.g., iDMRs *RIMBP3* and *CDRT15P6*) or when genes of interest fall inside inversions (e.g., *PMS2* in inversion chr7: 5850673–6795880).

DNA-methylation-based (canonical) imprinting has been described in all placental mammals, and genomic maps of iDMRs have been established for a number of species, notably mice and primates.^{10,45–47} Although our approach can potentially be expanded to other organisms, it would be limited to chromosomes with known iDMRs (e.g., not chromosomes 4, 5, 13, 14, 16, and 19 in mice).¹⁰ This would primarily require adjusting cell culture and flow cytometry conditions for Strand-seq library preparation to suit non-human cells.⁴⁸

STAR★METHODS

Detailed methods are provided in the online version of this paper and include the following:

- [KEY RESOURCES TABLE](#)
- [RESOURCE AVAILABILITY](#)
 - Lead contact
 - Materials availability
 - Data and code availability
- [EXPERIMENTAL MODEL AND SUBJECT DETAILS](#)
- [METHOD DETAILS](#)
 - Nanopore sequencing and data
 - Nanopore data analysis
 - Strand-seq phasing and inversion correction
 - iDMR selection

- Chromosome-scale haplotypes and PofO detection
- Mendelian errors
- **QUANTIFICATION AND STATISTICAL ANALYSIS**

SUPPLEMENTAL INFORMATION

Supplemental information can be found online at <https://doi.org/10.1016/j.xgen.2022.100233>.

ACKNOWLEDGMENTS

We thank Yanni Wang and Daniel Chan for help with making Strand-seq libraries. We are grateful for discussions related to inversion-aware phasing with David Porubsky. We thank Martin Krzywinski and Katherine Dixon for their work on the graphical abstract. V.A. acknowledges funding from the University of British Columbia Four Year Doctoral Fellowship. Work in the Lansdorp laboratory is funded by a Program Project Grant (#1074) from the Terry Fox Research Institute; a Project Grant (#PJT-159787) from the Canadian Institutes of Health Research; and a grant (#40044) from the Canadian Foundation for Innovation and the government of British Columbia. L.L. acknowledges funding from a Project Grant (#PJT-165992) from the Canadian Institutes of Health Research. K.A.S. acknowledges funding from the Canada Research Chairs program and Canadian Institutes of Health Research. S.J.M.J. acknowledges funding from the Canada Research Chairs program and the Canadian Foundation for Innovation.

AUTHOR CONTRIBUTIONS

Conceptualization and methodology, all authors; software, validation, visualization, and writing – original draft, V.A. and V.C.T.H.; writing – review & editing, all authors.

DECLARATION OF INTERESTS

The authors declare no competing interests.

Received: May 20, 2022

Revised: September 8, 2022

Accepted: November 29, 2022

Published: December 21, 2022

REFERENCES

1. Zheng, G.X.Y., Lau, B.T., Schnall-Levin, M., Jarosz, M., Bell, J.M., Hindson, C.M., Kyriazopoulou-Panagiotopoulou, S., Masquelier, D.A., Merrill, L., Terry, J.M., et al. (2016). Haplotyping germline and cancer genomes with high-throughput linked-read sequencing. *Nat. Biotechnol.* *34*, 303–311.
2. Wenger, A.M., Peluso, P., Rowell, W.J., Chang, P.-C., Hall, R.J., Conception, G.T., Ebler, J., Fungtammasan, A., Kolesnikov, A., Olson, N.D., et al. (2019). Accurate circular consensus long-read sequencing improves variant detection and assembly of a human genome. *Nat. Biotechnol.* *37*, 1155–1162.
3. Cheng, H., Jarvis, E.D., Fedrigo, O., Koepfli, K.-P., Urban, L., Gemmell, N.J., and Li, H. (2022). Haplotype-resolved assembly of diploid genomes without parental data. *Nat. Biotechnol.* *40*, 1332–1335. <https://doi.org/10.1038/s41587-022-01261-x>.
4. Jarvis, E.D., Formenti, G., Rhie, A., Guarracino, A., Yang, C., Wood, J., Tracey, A., Thibaud-Nissen, F., Vollger, M.R., Porubsky, D., et al. (2022). Automated assembly of high-quality diploid human reference genomes. Preprint at bioRxiv. <https://doi.org/10.1101/2022.03.06.483034>.
5. Henckel, A., and Arnaud, P. (2010). Genome-wide identification of new imprinted genes. *Brief. Funct. Genomics* *9*, 304–314.
6. Zink, F., Magnusdottir, D.N., Magnusson, O.T., Walker, N.J., Morris, T.J., Sigurdsson, A., Halldorsson, G.H., Gudjonsson, S.A., Melsted, P., Ingimundardottir, H., et al. (2018). Insights into imprinting from parent-of-origin phased methylomes and transcriptomes. *Nat. Genet.* *50*, 1542–1552.
7. Laszlo, A.H., Derrington, I.M., Brinkerhoff, H., Langford, K.W., Nova, I.C., Samson, J.M., Bartlett, J.J., Pavlenok, M., and Gundlach, J.H. (2013). Detection and mapping of 5-methylcytosine and 5-hydroxymethylcytosine with nanopore MspA. *Proc. Natl. Acad. Sci. USA* *110*, 18904–18909.
8. Simpson, J.T., Workman, R.E., Zuzarte, P.C., David, M., Dursi, L.J., and Timp, W. (2017). Detecting DNA cytosine methylation using nanopore sequencing. *Nat. Methods* *14*, 407–410.
9. Akbari, V., Garant, J.-M., O'Neill, K., Pandoh, P., Moore, R., Marra, M.A., Hirst, M., and Jones, S.J.M. (2021). Megabase-scale methylation phasing using nanopore long reads and NanoMethPhase. *Genome Biol.* *22*, 68.
10. Gigante, S., Gouil, Q., Lucattini, A., Keniry, A., Beck, T., Tinning, M., Gordon, L., Woodruff, C., Speed, T.P., Blewitt, M.E., et al. (2019). Using long-read sequencing to detect imprinted DNA methylation. *Nucleic Acids Res.* *47*, e46.
11. Porubský, D., Sanders, A.D., van Wietmarschen, N., Falconer, E., Hills, M., Spierings, D.C.J., Bevova, M.R., Guryev, V., and Lansdorp, P.M. (2016). Direct chromosome-length haplotyping by single-cell sequencing. *Genome Res.* *26*, 1565–1574.
12. Selvaraj, S., R Dixon, J., Bansal, V., and Ren, B. (2013). Whole-genome haplotype reconstruction using proximity-ligation and shotgun sequencing. *Nat. Biotechnol.* *31*, 1111–1118.
13. Falconer, E., Hills, M., Naumann, U., Poon, S.S.S., Chavez, E.A., Sanders, A.D., Zhao, Y., Hirst, M., and Lansdorp, P.M. (2012). DNA template strand sequencing of single-cells maps genomic rearrangements at high resolution. *Nat. Methods* *9*, 1107–1112.
14. Porubsky, D., Garg, S., Sanders, A.D., Korbelt, J.O., Guryev, V., Lansdorp, P.M., and Marschall, T. (2017). Dense and accurate whole-chromosome haplotyping of individual genomes. *Nat. Commun.* *8*, 1293.
15. Porubsky, D., Ebert, P., Audano, P.A., Vollger, M.R., Harvey, W.T., Marijon, P., Ebler, J., Munson, K.M., Sorensen, M., Sulovari, A., et al. (2021). Fully phased human genome assembly without parental data using single-cell strand sequencing and long reads. *Nat. Biotechnol.* *39*, 302–308.
16. Chaisson, M.J.P., Sanders, A.D., Zhao, X., Malhotra, A., Porubsky, D., Rausch, T., Gardner, E.J., Rodriguez, O.L., Guo, L., Collins, R.L., et al. (2019). Multi-platform discovery of haplotype-resolved structural variation in human genomes. *Nat. Commun.* *10*, 1784.
17. Ebert, P., Audano, P.A., Zhu, Q., Rodriguez-Martin, B., Porubsky, D., Bonder, M.J., Sulovari, A., Ebler, J., Zhou, W., Serra Mari, R., et al. (2021). Haplotype-resolved diverse human genomes and integrated analysis of structural variation. *Science* *372*. eabf7117.
18. van der Mey, A.G., Maaswinkel-Mooy, P.D., Cornelisse, C.J., Schmidt, P.H., and van de Kamp, J.J. (1989). Genomic imprinting in hereditary glomus tumours: evidence for new genetic theory. *Lancet* *2*, 1291–1294.
19. Knowles, J.W., Rader, D.J., and Khoury, M.J. (2017). Cascade screening for familial hypercholesterolemia and the use of genetic testing. *JAMA* *318*, 381–382.
20. Richards, S., Aziz, N., Bale, S., Bick, D., Das, S., Gastier-Foster, J., Grody, W.W., Hegde, M., Lyon, E., Spector, E., et al. (2015). Standards and guidelines for the interpretation of sequence variants: a joint consensus recommendation of the American college of medical genetics and genomics and the association for molecular pathology. *Genet. Med.* *17*, 405–424.
21. Hensen, E.F., Jordanova, E.S., van Minderhout, I.J.H.M., Hogendoorn, P.C.W., Taschner, P.E.M., van der Mey, A.G.L., Devilee, P., and Cornelisse, C.J. (2004). Somatic loss of maternal chromosome 11 causes parent-of-origin-dependent inheritance in SDHD-linked paraganglioma and pheochromocytoma families. *Oncogene* *23*, 4076–4083.
22. Hao, H.X., Khalimonchuk, O., Schraders, M., Dephoure, N., Bayley, J.P., Kunst, H., Devilee, P., Cremers, C.W.R.J., Schiffman, J.D., Bentz, B.G., et al. (2009). SDH5, a gene required for flavination of succinate dehydrogenase, is mutated in paraganglioma. *Science* *325*, 1139–1142.

23. Hampel, H. (2016). Genetic counseling and cascade genetic testing in Lynch syndrome. *Fam. Cancer* *15*, 423–427.
24. Lee, P.W.C., Bedard, A.C., Samimi, S., Beard, V.K., Hong, Q., Bedard, J.E.J., Gilks, B., Schaeffer, D.F., Wolber, R., Kwon, J.S., et al. (2020). Evaluating the impact of universal Lynch syndrome screening in a publicly funded healthcare system. *Cancer Med.* *9*, 6507–6514.
25. Braley, E.F., Bedard, A.C., Nuk, J., Hong, Q., Bedard, J.E.J., Sun, S., and Schrader, K.A. (2022). Patient ethnicity and cascade genetic testing: a descriptive study of a publicly funded hereditary cancer program. *Cancer* *21*, 369–374. <https://doi.org/10.1007/s10689-021-00270-0>.
26. Zook, J.M., McDaniel, J., Olson, N.D., Wagner, J., Parikh, H., Heaton, H., Irvine, S.A., Trigg, L., Truty, R., McLean, C.Y., et al. (2019). An open resource for accurately benchmarking small variant and reference calls. *Nat. Biotechnol.* *37*, 561–566.
27. 1000 Genomes Project Consortium; Auton, A., Brooks, L.D., Durbin, R.M., Garrison, E.P., Kang, H.M., Korbel, J.O., Marchini, J.L., McCarthy, S., McVean, G.A., et al. (2015). A global reference for human genetic variation. *Nature* *526*, 68–74.
28. Zheng, Z., Li, S., Su, J., Leung, A.W.-S., Lam, T.-W., and Luo, R. (2021). Symphonizing pileup and full-alignment for deep learning-based long-read variant calling. Preprint at bioRxiv. <https://doi.org/10.1101/2021.12.29.474431>.
29. Court, F., Tayama, C., Romanelli, V., Martin-Trujillo, A., Iglesias-Platas, I., Okamura, K., Sugahara, N., Simón, C., Moore, H., Harness, J.V., et al. (2014). Genome-wide parent-of-origin DNA methylation analysis reveals the intricacies of human imprinting and suggests a germline methylation-independent mechanism of establishment. *Genome Res.* *24*, 554–569.
30. Joshi, R.S., Garg, P., Zaitlen, N., Lappalainen, T., Watson, C.T., Azam, N., Ho, D., Li, X., Antonarakis, S.E., Brunner, H.G., et al. (2016). DNA methylation profiling of uniparental disomy subjects provides a map of parental epigenetic bias in the human genome. *Am. J. Hum. Genet.* *99*, 555–566.
31. Hernandez Mora, J.R., Tayama, C., Sánchez-Delgado, M., Monteagudo-Sánchez, A., Hata, K., Ogata, T., Medrano, J., Poo-Llanillo, M.E., Simón, C., Moran, S., et al. (2018). Characterization of parent-of-origin methylation using the Illumina Infinium MethylationEPIC array platform. *Epigenomics* *10*, 941–954.
32. Akbari, V., Garant, J.-M., O'Neill, K., Pandoh, P., Moore, R., Marra, M.A., Hirst, M., and Jones, S.J.M. (2022). Genome-wide detection of imprinted differentially methylated regions using nanopore sequencing. *Elife* *11*, e77898.
33. Jain, M., Koren, S., Miga, K.H., Quick, J., Rand, A.C., Sasani, T.A., Tyson, J.R., Beggs, A.D., Dilthey, A.T., Fiddes, I.T., et al. (2018). Nanopore sequencing and assembly of a human genome with ultra-long reads. *Nat. Biotechnol.* *36*, 338–345.
34. Miller, D.T., Lee, K., Chung, W.K., Gordon, A.S., Herman, G.E., Klein, T.E., Stewart, D.R., Amendola, L.M., Adelman, K., Bale, S.J., et al. (2021). ACMG SF v3.0 list for reporting of secondary findings in clinical exome and genome sequencing: a policy statement of the American College of Medical Genetics and Genomics (ACMG). *Genet. Med.* *23*, 1381–1390.
35. Offit, K., Tkachuk, K.A., Stadler, Z.K., Walsh, M.F., Diaz-Zabala, H., Levin, J.D., Steinsnyder, Z., Ravichandran, V., Sharaf, R.N., Frey, M.K., et al. (2020). Cascading after peridiagnostic cancer genetic testing: an alternative to population-based screening. *J. Clin. Oncol.* *38*, 1398–1408.
36. Garg, S., Fungtammasan, A., Carroll, A., Chou, M., Schmitt, A., Zhou, X., Mac, S., Peluso, P., Hatas, E., Ghurye, J., et al. (2021). Chromosome-scale, haplotype-resolved assembly of human genomes. *Nat. Biotechnol.* *39*, 309–312.
37. Tse, O.Y.O., Jiang, P., Cheng, S.H., Peng, W., Shang, H., Wong, J., Chan, S.L., Poon, L.C.Y., Leung, T.Y., Chan, K.C.A., et al. (2021). Genome-wide detection of cytosine methylation by single molecule real-time sequencing. *Proc. Natl. Acad. Sci. USA* *118*. e2019768118.
38. Hanlon, V.C.T., Chan, D.D., Hamadeh, Z., Wang, Y., Mattsson, C.-A., Spierings, D.C.J., Coope, R.J.N., and Lansdorp, P.M. (2022). Construction of Strand-seq libraries in open nanoliter arrays. *Cell Rep. Methods* *2*, 100150.
39. Ledford, H. (2019). Cancer geneticists tackle troubling ethnic bias in studies. *Nature* *568*, 154–155. <https://doi.org/10.1038/d41586-019-01080-2>.
40. Prickett, A.R., and Oakey, R.J. (2012). A survey of tissue-specific genomic imprinting in mammals. *Mol. Genet. Genomics.* *287*, 621–630.
41. Monk, D., Mackay, D.J.G., Eggermann, T., Maher, E.R., and Riccio, A. (2019). Genomic imprinting disorders: lessons on how genome, epigenome and environment interact. *Nat. Rev. Genet.* *20*, 235–248.
42. Jima, D.D., Skaar, D.A., Planchart, A., Motsinger-Reif, A., Cevik, S.E., Park, S.S., Cowley, M., Wright, F., House, J., Liu, A., et al. (2022). Genomic map of candidate human imprint control regions: the imprintome. *Epigenetics* *17*, 1920–1943. <https://doi.org/10.1080/15592294.2022.2091815>.
43. Shafin, K., Pesout, T., Chang, P.-C., Nattestad, M., Kolesnikov, A., Goel, S., Baid, G., Kolmogorov, M., Eizenga, J.M., Miga, K.H., et al. (2021). Haplotype-aware variant calling with PEPPER-Margin-DeepVariant enables high accuracy in nanopore long-reads. *Nat. Methods* *18*, 1322–1332.
44. Porubsky, D., Höps, W., Ashraf, H., Hsieh, P., Rodriguez-Martin, B., Yilmaz, F., Ebler, J., Hallast, P., Maria Maggolini, F.A., Harvey, W.T., et al. (2022). Recurrent inversion polymorphisms in humans associate with genetic instability and genomic disorders. *Cell* *185*, 1986–2005.e26.
45. Renfree, M.B., Hore, T.A., Shaw, G., Graves, J.A.M., and Pask, A.J. (2009). Evolution of genomic imprinting: insights from marsupials and monotremes. *Annu. Rev. Genomics Hum. Genet.* *10*, 241–262.
46. Cheong, C.Y., Chng, K., Ng, S., Chew, S.B., Chan, L., and Ferguson-Smith, A.C. (2015). Germline and somatic imprinting in the nonhuman primate highlights species differences in oocyte methylation. *Genome Res.* *25*, 611–623.
47. Xie, W., Barr, C.L., Kim, A., Yue, F., Lee, A.Y., Eubanks, J., Dempster, E.L., and Ren, B. (2012). Base-Resolution analyses of sequence and parent-of-origin dependent DNA methylation in the mouse genome. *Cell* *148*, 816–831.
48. Hills, M., Falconer, E., O'Neill, K., Sanders, A.D., Howe, K., Guryev, V., and Lansdorp, P.M. (2021). Construction of whole genomes from scaffolds using single cell strand-seq data. *Int. J. Mol. Sci.* *22*, 3617.
49. De Coster, W., De Rijk, P., De Roeck, A., De Pooter, T., D'Hert, S., Straziarsar, M., Slegers, K., and Van Broeckhoven, C. (2019). Structural variants identified by Oxford Nanopore PromethION sequencing of the human genome. *Genome Res.* *29*, 1178–1187.
50. Gamaarachchi, H., Lam, C.W., Jayatilaka, G., Samarakoon, H., Simpson, J.T., Smith, M.A., and Parameswaran, S. (2020). GPU accelerated adaptive banded event alignment for rapid comparative nanopore signal analysis. *BMC Bioinf.* *21*, 343.
51. Eimer, C., Sanders, A.D., Korbel, J.O., Marschall, T., and Ebert, P. (2021). ASHLEYS: automated quality control for single-cell Strand-seq data. *Bioinformatics* *37*, 3356–3357.
52. Porubsky, D., Sanders, A.D., Taudt, A., Colomé-Tatché, M., Lansdorp, P.M., and Guryev, V. (2020). breakpointR: an R/Bioconductor package to localize strand state changes in Strand-seq data. *Bioinformatics* *36*, 1260–1261.
53. Hanlon, V.C.T., Mattsson, C.-A., Spierings, D.C.J., Guryev, V., and Lansdorp, P.M. (2021). InverttypeR: bayesian inversion genotyping with Strand-seq data. *BMC Genom.* *22*, 582.
54. Wang, T., Antonacci-Fulton, L., Howe, K., Lawson, H.A., Lucas, J.K., Philipp, A.M., Popejoy, A.B., Asri, M., Carson, C., Chaisson, M.J.P., et al. (2022). The Human Pangenome Project: a global resource to map genomic diversity. *Nature* *604*, 437–446.
55. Li, H. (2018). Minimap2: pairwise alignment for nucleotide sequences. *Bioinformatics* *34*, 3094–3100.

56. Akbari, V., Garant, J.-M., O'Neill, K., Pandoh, P., Moore, R., Marra, M., Hirst, M., and Jones, S. (2021). NanoMethPhase (Zenodo). <https://doi.org/10.5281/zenodo.4474430>.
57. Wagner, J., Olson, N.D., Harris, L., Khan, Z., Farek, J., Mahmoud, M., Stankovic, A., Kovacevic, V., Yoo, B., Miller, N., et al. (2022). Benchmarking challenging small variants with linked and long reads. *Cell Genom.* 2, 100128.
58. Martin, M. (2011). Cutadapt removes adapter sequences from high-throughput sequencing reads. *EMBnet J.* 17, 10.
59. Langmead, B., and Salzberg, S.L. (2012). Fast gapped-read alignment with Bowtie 2. *Nat. Methods* 9, 357–359.
60. Stunnenberg, H.G., International Human Epigenome Consortium; Hirst, M., de Almeida, M., Altucci, L., Amin, V., Amit, I., Antonarakis, S.E., and Hirst, M. (2016). The international human epigenome consortium: a Blueprint for scientific collaboration and discovery. *Cell* 167, 1145–1149.
61. ENCODE Project Consortium (2012). An integrated encyclopedia of DNA elements in the human genome. *Nature* 489, 57–74.
62. Bernstein, B.E., Stamatoyannopoulos, J.A., Costello, J.F., Ren, B., Milosavljevic, A., Meissner, A., Kellis, M., Marra, M.A., Beaudet, A.L., Ecker, J.R., et al. (2010). The NIH roadmap epigenomics mapping consortium. *Nat. Biotechnol.* 28, 1045–1048.
63. Byrska-Bishop, M., Evani, U.S., Zhao, X., Basile, A.O., Abel, H.J., Regier, A.A., Corvelo, A., Clarke, W.E., Musunuri, R., Nagulapalli, K., et al. (2021). High coverage whole genome sequencing of the expanded 1000 Genomes Project cohort including 602 trios. Preprint at bioRxiv. <https://doi.org/10.1101/2021.02.06.430068>.
64. Hao, Z., Lv, D., Ge, Y., Shi, J., Weijers, D., Yu, G., and Chen, J. (2020). RIdiogram: drawing SVG graphics to visualize and map genome-wide data on the idiograms. *PeerJ. Comput. Sci.* 6, e251.

STAR★METHODS

KEY RESOURCES TABLE

REAGENT or RESOURCE	SOURCE	IDENTIFIER
Critical commercial assays		
Ligation sequencing kit	Oxford Nanopore Technologies	Cat. #: SQK-LSK109
PromethION R9.4.1 pore flow cell	Oxford Nanopore Technologies	Cat. #: FLO-PRO002
Deposited data		
HG002 nanopore FAST5 files	This study	SRA: SRP395905
HG005 and HG00733 nanopore FAST5 files	The Human Pangenome Reference Consortium	s3-us-west-2.amazonaws.com/human-pangenomics/index.html?prefix=NHGRI_UCSC_panel/
NA12878 nanopore FAST5 files	Ref. Jain et al., ³³	nanopore-wgs-consortium NA12878 rel6 https://github.com/nanopore-wgs-consortium/NA12878
NA19240 nanopore FAST5 files	Ref. De Coster et al., ⁴⁹	ENA: PRJEB26791
HG002 and HG005 Strand-seq FASTQ files	The Genome in a Bottle Consortium	ftp-trace.ncbi.nlm.nih.gov/ReferenceSamples/giab/data/
HG00733 and NA19240 Strand-seq FASTQ files	The Human Genome Structural Variation Consortium	www.internationalgenome.org/
NA12878 Strand-seq FASTQ files	Ref. Hanlon et al., ³⁸	SRA: SRP326369; BioProject: PRJNA742746
PofO phased VCF files	This study	https://doi.org/10.5281/zenodo.7052113
Experimental models: Cell lines		
Human: EBV-transformed B cells for GM24385 Coriell RRID: CVCL_7526	Coriell	CVCL_1C78
Software and algorithms		
Clair3 v0.1-r10	Ref. Zheng et al., ²⁸	N/A
f5c v0.6	Ref. Gamaarachchi et al., ⁵⁰	N/A
Nanopolish v0.13.3	Ref. Simpson et al., ⁸	N/A
NanoMethPhase v1.0	Ref. Akbari et al., ⁹	https://doi.org/10.5281/zenodo.4474430
ASHLEYS QC	Ref. Eimer et al., ⁵¹	N/A
BreakpointR	Ref. Porubsky et al., ⁵²	GitHub: daewoooo/breakpointR commit 58cce0b09d01040892b3f6abf0b11caeb403d3f5
StrandPhaseR	Ref. Porubsky et al., ¹⁴	GitHub: daewoooo/StrandPhaseR commit bb19557235de3d82092abdc11b3334f615525b5b
InvertypeR	Ref. Hanlon et al., ⁵³	N/A
correctInvertedRegionPhasing	Ref. Porubsky et al., ⁴⁴	N/A
PatMat v1.1.1	This study	https://doi.org/10.5281/zenodo.7308808 ; GitHub: https://github.com/vahidAK/PatMat

RESOURCE AVAILABILITY

Lead contact

Further information and requests for resources and reagents should be directed to and will be fulfilled by the lead contact, Dr. Steven J.M. Jones (sjones@bcgsc.ca).

Materials availability

This study did not generate new unique reagents.

Data and code availability

- Nanopore data for HG002 have been deposited at the NCBI Sequence Read Archive and are publicly available as of the date of publication (SRA: SRP395905). Phased variant call files are also deposited at Zenodo (<https://doi.org/10.5281/zenodo.7052113>). The accession numbers are also listed in the [key resources table](#).
- All original code has been deposited at Zenodo (<https://doi.org/10.5281/zenodo.7308808>) and on GitHub (<https://github.com/vahidAK/PatMat>) and is publicly available. Tools and DOIs are also listed in the [key resources table](#).
- Any additional information required to reanalyze the data reported in this paper is available from the [lead contact](#) upon request.

EXPERIMENTAL MODEL AND SUBJECT DETAILS

NA12878: female, age unknown. HG002: male, 45 years. HG005: male, 33 years. HG00733: female, age unknown. NA19240: female, age unknown. This study involved five trios, and PofO was assigned for the five children. HG002 cells were purchased from Coriell for nanopore sequencing. They were cultured in RPMI 1640 medium supplemented with 15% FBS (not heat inactivated) at 37°C with 5% CO₂ at a density of 10⁶ cells/mL with a split ratio of 1:4. The cell line was not authenticated, except insofar as HG002's small variant haplotypes match those of his parents ([Figure S13](#)).

METHOD DETAILS

Nanopore sequencing and data

We sequenced native DNA from an Ashkenazi son (GM24385, or HG002) at 33-fold coverage. We first extracted high molecular weight genomic DNA from an EBV-transformed B-lymphocyte cell line and sheared it to an average size of 6–20 kb using g-TUBE shearing (Covaris). We then repaired potential nicks using the NEBNext FFPE DNA Repair kit (PreCR treatment) and performed end-repair and A-tailing using the NEBNext Ultra II kit. We ligated to the Oxford Nanopore Technologies adapters using NEBNext Quick Ligase, and we removed small library fragments using a 0.4:1 bead:library ratio. We sequenced the library on an Oxford Nanopore Technologies PromethION 24 instrument using an R9.4.1 pore flow cell and software version 19.06.9 (MinKNOW GUI v4.0.23). A nuclease flush was performed after 48 h of sequencing and prior to library re-loading for a further 24 h.

In addition to HG002, we used public nanopore data for HG005, HG00733, NA12878 and NA19240 ([Figure S1](#)). Raw nanopore fast5 files for HG005 and HG00733 were downloaded from the Human Pangenome Reference Consortium⁵⁴ (<https://github.com/human-pangenomics>); NA12878 was obtained from Jain et al. 2018³³; and NA19240 from De Coster et al. 2019.⁴⁹ For HG002, HG005 and NA12878, ground truth phased variants were obtained through GIAB v4.2.1 (hifiasm_v11_phasetransfer), and for NA19240 and HG00733 phased variants were obtained from 1KGP shapeit2 v2a (shapeit2_integrated_snvindels_v2a_related_samples).^{26,27}

Nanopore data analysis

Base calling and mapping

Nanopore signal-level data were basecalled using Oxford Nanopore Technologies guppy basecaller v6.0.1 and the super accuracy model (dna_r9.4.1_450bps_sup) with default settings. Basecalled nanopore reads were mapped to the human reference genome (GRCh38; with the EBV genome but no ALT contigs) using minimap2 v2.24 with the *-ax map-ont -MD -L* options selected.⁵⁵

Variant calling

Upon alignment, Clair3 v0.1-r10 with trained model r941_prom_sup_g5014 and default settings was used to call variants from nanopore alignment data.²⁸ High quality variant calls (marked as “PASS” by the software) from Clair3 were then used for Strand-seq phasing (see the next section).

Methylation calling

To call DNA methylation and obtain per-read CpG methylation information from nanopore data, we first indexed fastq file using f5c v0.6⁵⁰ and then called methylation using nanopolish v0.13.3 with default settings⁹. Per-read methylation call data were then preprocessed using NanoMethPhase v1.0 methyl_call_processor module with *-callThreshold 1.5* for downstream analysis and PofO phasing.^{9,56}

Strand-seq phasing and inversion correction

We obtained 45 public Strand-seq libraries for HG005 and 66 for HG002 from GIAB^{26,57} (<ftp-trace.ncbi.nlm.nih.gov/ReferenceSamples/giab/data/>), and we obtained 230 libraries for HG00733 and 234 libraries for NA19240 from HGVC.¹⁶ We used the 96 high-depth OP-Strand-seq libraries for NA12878 described previously (clusters 5 and 6).³⁸

We trimmed adapters from paired-end FASTQ files and removed short reads (<30 bp) and low-quality bases (<15) with Cutadapt.⁵⁸ We used Bowtie2 to align reads to the GRCh38 human reference genome and discarded reads that had MAPQ less than 10 or that did

not map to chromosomes 10–22, X, and Y.⁵⁹ We used Picard to mark duplicate reads (github.com/broadinstitute/picard/) and then ran ASHLEYS QC with default settings and window sizes 5000000, 2000000, 1000000, 800000, 600000, 400000, and 200000 to discard libraries with a Strand-seq quality score below 0.5.⁵¹

We ran BreakpointR (commit 58cce0b09d01040892b3f6abf0b11caeb403d3f5 of github.com/daewoooo/breakpointR) with background set to 0.1, chr set to the autosomes, and maskRegions set to a previously described blacklist.^{52,53} We used 8 Mb bins because we found they linked phasing across difficult regions such as inversions more readily and prevented large switch errors (Figure 4D). We used the function exportRegions with default settings to identify regions of the genome with both Watson and Crick reads that are suitable for phasing. We phased biallelic heterozygous SNVs called from the nanopore data for each sample using StrandPhaseR with num.iterations set to 3, with splitPhasedReads and assume.biallelic set to TRUE, with R v4.0.5, and with v1.0.1 or higher of the dependency rlang (commit bb19557235de3d82092abdc11b3334f615525b5b of the devel branch of github.com/daewoooo/StrandPhaseR).¹⁴

Inversions disrupt Strand-seq's directional phase information. We called inversions for each sample using the R package InverttypeR (commit a5fac3b6b8264db28de1a997ad0bc062badea883 of github.com/vincent-hanlon/InverttypeR/commits/main).⁵³ In brief, we used the nanopore SNVs to create a pair of composite files for each sample, with the addition of the genomic coordinates chr8:8231088–12039415 in the blacklist to ensure that the common large inversion at those coordinates was correctly represented. We genotyped a catalog of published inversion coordinates with adjust_method set to 'all' and with priors as previously described, as well as a list of *de novo* sample-specific strand switches identified by running BreakpointR three times on the composite files with different bin sizes.^{52,53} For the latter, we used prior probabilities of 0.9, 0.05, and 0.05 for reference, heterozygous, and homozygous genotypes, respectively. We combined inversions with posterior probabilities above 0.95 from the two callsets by discarding any inversions from the catalog callset that intersected the *de novo* callset (`bedtools intersect -v -r -f 0.1`). We did not remove misoriented reference contigs, which appear as homozygous inversions in all samples, because they disrupt phasing in the same way that inversions do.

The function correctInvertedRegionPhasing in the StrandPhaseR package switches the phase of heterozygous SNVs within homozygous inversions and re-phases SNVs within heterozygous inversions.⁴⁴ We used sample-specific inversion calls larger than 10 kb along with the nanopore sample-specific SNV positions, recall.phased and assume.biallelic set to TRUE, het.genotype set to 'lenient', lookup.bp set to 1000000, background set to 0.1, and lookup.blacklist set to the blacklist above. The resulting chromosome-length inversion-corrected SNV haplotypes were used to phase nanopore reads relative to each other.

iDMR selection

We gathered the list of previously reported iDMRs from five prior genome-wide studies.^{6,29–32} iDMRs with overlap between two or more studies were merged into the largest total interval. Moreover, iDMRs within 1 kb and with the same PoFO were merged. This resulted in 93 iDMRs reported in at least two studies and 306 iDMRs reported in only a single study and supported by at least two probes if they came from array studies. We previously surveyed imprinted methylation genome-wide using 12 nanopore-sequenced cell lines with their trio sequencing information from 1KGP.³² We used the same cell lines to examine the 306 iDMRs from a single study, above. At each allele for each CpG site with coverage >4× within the iDMRs, methylation frequency (the fraction of reads methylated at a CpG) was calculated. We then calculated the difference between average methylation frequencies for the paternal and maternal alleles for each iDMR in each cell line. Ninety-four iDMRs with $|methylation\ difference| \geq 0.25$ between alleles and with conflicting PoFO between any of the 12 cell lines and the corresponding prior study were excluded. To further validate the 212 remaining iDMRs reported in a single study, we used WGBS datasets for 119 blood samples from 87 individuals in the Blueprint consortium and 60 tissue samples for 29 tissue types in ENCODE and the RoadMap consortium^{60–62} (Tables S5 and S6). At iDMRs only one allele is methylated, therefore, the aggregated methylation frequency from both alleles at these regions is expected to be ~50% (partial methylation). Thus, we examined partial methylation at the 212 iDMRs in the WGBS datasets. For each WGBS sample, we used CpGs with at least five mapped WGBS reads and at each iDMR we counted the number of CpGs with partial methylation (methylation frequency between 0.35 and 0.65 among mapped reads). An iDMR with 0.35–0.65 methylation is then considered partially methylated if it had at least five CpGs in the WGBS sample and more than 60% of the CpGs showed partial methylation (see similar requirements used elsewhere³²). We only included iDMRs that were partially methylated in at least two and 5% of individuals or tissues in which the iDMR could be examined (i.e., the iDMR had at least five CpGs with a coverage of ≥ 5). Out of the 212 iDMRs, 113 iDMRs were excluded because they did not meet the inclusion criteria, suggesting that they rarely provide parental information. Unlike true iDMRs, randomly selected loci are unlikely to meet these criteria. To test this, we randomly selected 100 genomic intervals with at least 15 CpGs and lengths of 1, 2, or 3 kb and repeated the experiment 100 times. On average, 2.4% of intervals met the inclusion criteria. Overall, we gathered a list of 192 known iDMRs of which 93 were reported in multiple studies and 99 were reported in a single study (Table S3).

Chromosome-scale haplotypes and PoFO detection

We then integrated several steps to detect chromosome-scale haplotypes with their PoFO.

1. Strand-seq phasing provides sparse chromosome-scale haplotypes. Phased SNVs from Strand-seq were used to phase nanopore reads to either HP1 or HP2 haplotypes. We used a minimum mapping quality of 20 and base quality of 7 to tag each read with the phased SNVs. We used somewhat similar criteria as NanoMethPhase⁹ to assign reads to haplotypes: we

- tag a read as HP1 if # HP1 SNVs > # HP2 SNVs in the read, the read has at least one phased SNV from HP1, and $(\# \text{ HP1 SNVs in the read} / \# \text{ all phased SNVs in the read}) \geq 0.75$, and vice versa.
2. Phased nanopore reads from step 1 were then used to re-phase all the variants (SNVs and indels) to each haplotype. Variants assigned to the haplotype supported by more reads and at least two phased reads needed to support a variant to assign it as HP1 or HP2.
 3. Nanopore reads were then phased a second time using all the phased variants from step 2 with the conditions mentioned in step 1.
 4. Per-read methylation information for each nanopore read at known iDMRs were extracted and integrated to its phase information from step 3. This enabled us to phase each CpG methylation in each read to either HP1 or HP2 and calculate the methylation frequency $(\# \text{ methylated reads} / \# \text{ all reads})$ at each CpG site for each haplotype. Methylation frequencies were then used to assign haplotypes to their PofO for each sample as follows:

At each of the 192 known iDMRs we considered CpGs detected in both haplotypes and counted CpGs with ≥ 0.35 difference in methylation frequency between haplotypes (differential methylation). Tuning this parameter by trial and error allowed us to identify informative CpGs while avoiding erroneous differential methylation. We then calculated the contribution/detection value of the iDMR to the PofO detection of each haplotype as follows:

$$X_{HP1} = m_{HP1} \frac{a_{HP1}}{n}$$

$$X_{HP2} = m_{HP2} \frac{a_{HP2}}{n}$$

where m_i is the average methylation frequency for the haplotype, a_i is the number of differentially methylated CpGs that support PofO for the haplotype, and n is the number of all CpGs at the iDMR. For maternally methylated iDMRs, X_{HP1} indicates the contribution value for HP1 as the maternal and HP2 as the paternal allele and X_{HP2} indicates the contribution value for HP2 as the maternal and HP1 as the paternal allele, vice versa for paternally methylated iDMRs. The length of an iDMR can vary between individuals, and different studies report different start and end positions for the same iDMR. We wished to capture PofO information even when just a small part of an iDMR is imprinted in an individual, while avoiding inferences based on very few CpGs. Therefore, we only used iDMRs with $|a_{HP1} - a_{HP2}|$ comprising at least 10% of all detected CpGs and with more than 11 detected CpGs in total (i.e., $\frac{|a_{HP1} - a_{HP2}|}{n} \geq 0.1$ and $n > 11$). As an example, for a maternally methylated iDMR with 20 CpGs detected in both haplotypes and 0.8 average methylation frequency at HP1 and 0.3 at HP2, if 12 CpGs show ≥ 0.35 methylation in HP1 compared to HP2 and two CpGs show ≥ 0.35 methylation in HP2 compared to HP1, then:

X_{HP1} for HP1 as maternal and HP2 as paternal is $X_{HP1} = (0.8 \times 12)/20$, and X_{HP2} for HP2 as maternal and HP1 as paternal is $X_{HP2} = (0.3 \times 2)/20$.

On each chromosome for each haplotype as being maternal or paternal, the value of $X = \sum x$ will be (similarly for HP2):

$$X_{HP1(\text{paternal})} = \sum_{j=1}^k X_{HP1(\text{paternal})j}$$

$$X_{HP1(\text{maternal})} = \sum_{j=1}^k X_{HP1(\text{maternal})j}$$

Where k is the number of iDMRs considered for the chromosome. If, for example, $X_{HP1(\text{maternal})}$ (i.e., $X_{HP2(\text{paternal})}$) is greater than $X_{HP2(\text{maternal})}$ (i.e., $X_{HP1(\text{paternal})}$) then HP1 is the maternal homolog and HP2 is the paternal homolog and we calculated the confidence score for PofO assignment of the chromosome as follows:

$$\frac{X_{HP1(\text{maternal})}}{(X_{HP1(\text{maternal})} + X_{HP2(\text{maternal})})}$$

5. Finally, phased variants from step 2 were assigned to their PofO with the results from step 4.

All the steps are integrated into our workflow and tool, PatMat, and a tutorial is provided on GitHub (<https://github.com/vahidAK/PatMat>; Zenodo: <https://doi.org/10.5281/zenodo.7308808>).

Mendelian errors

To verify the PofO assignments, we calculated the frequency of one kind of Mendelian error between the PofO-assigned haplotypes and the genotypes of the parents. We obtained genotypes from GIAB for the parents of HG002 and HG005 (v4.2.1), from 1KGP for the parents of HG00733 and NA19240 (v2a), and from Byrska-Bishop et al. 2021 for the parents of NA12878.^{26,27,57,63} For each parent-child pair, we examined loci at which we found a phased heterozygous genotype for the child and either a heterozygous or

homozygous alternate genotype for the parent. Where the child had a maternal reference allele and the mother was homozygous alternate, we called a Mendelian error (similarly for the child's paternal allele and the father's genotype). We did this for non-overlapping bins of 1000 variants and calculated the error rate as the number of such Mendelian errors divided by the number of variants examined. We plotted the resulting error rates on chromosomes using RIdeogram.⁶⁴

QUANTIFICATION AND STATISTICAL ANALYSIS

PofO phasing was validated for 110 chromosomes from 5 individuals. No statistical tests were performed. However, we report non-probabilistic confidence scores that reflect the strength of differential methylation for each chromosome.

Cell Genomics, Volume 3

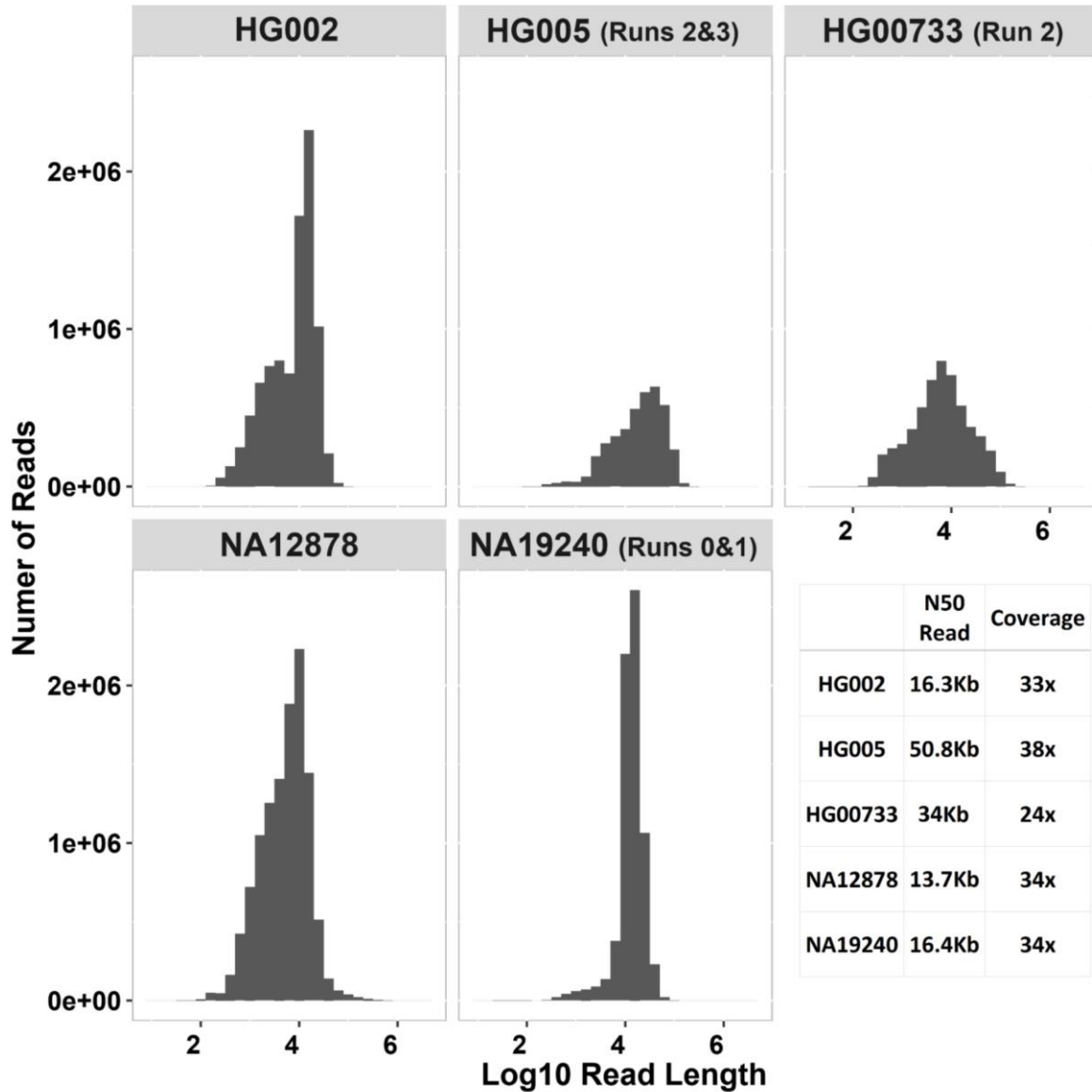
Supplemental information

Parent-of-origin detection and chromosome-scale

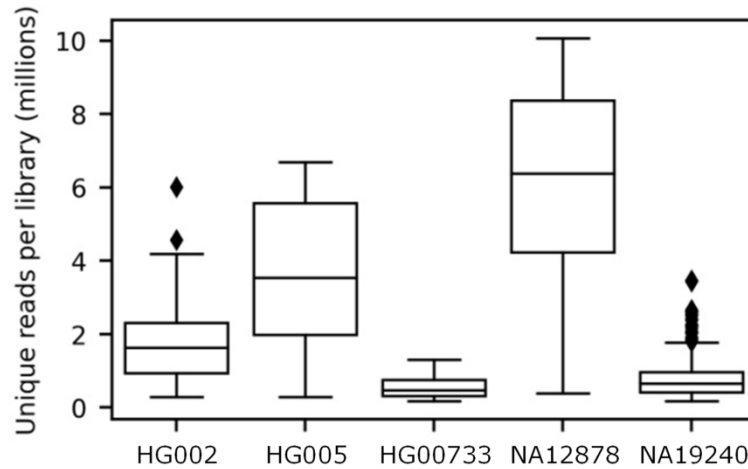
haplotyping using long-read DNA

methylation sequencing and Strand-seq

Vahid Akbari, Vincent C.T. Hanlon, Kieran O'Neill, Louis Lefebvre, Kasmintan A. Schrader, Peter M. Lansdorp, and Steven J.M. Jones

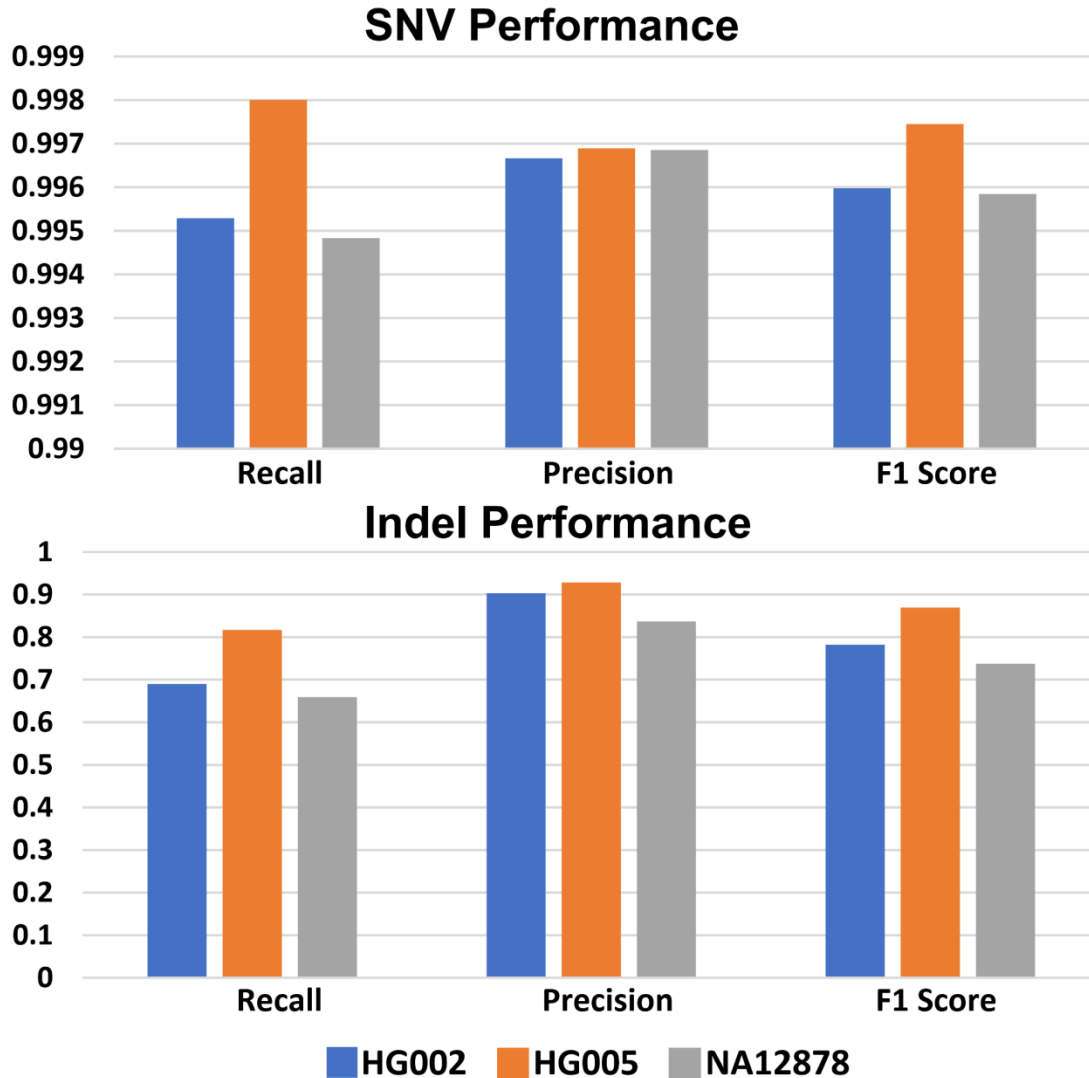


Supplementary Figure S1. Nanopore samples and their read distribution, N50 read length and coverage. Only guppy basecalling quality passed reads were used for downstream analysis. For HG005, HG00733 and NA19240, “Run” specifies the sequencing runs from public data that were used in our study. Related to the Results “Nanopore and Strand-seq enable chromosome-scale haplotyping” section and STAR Methods “Nanopore sequencing and data” section.

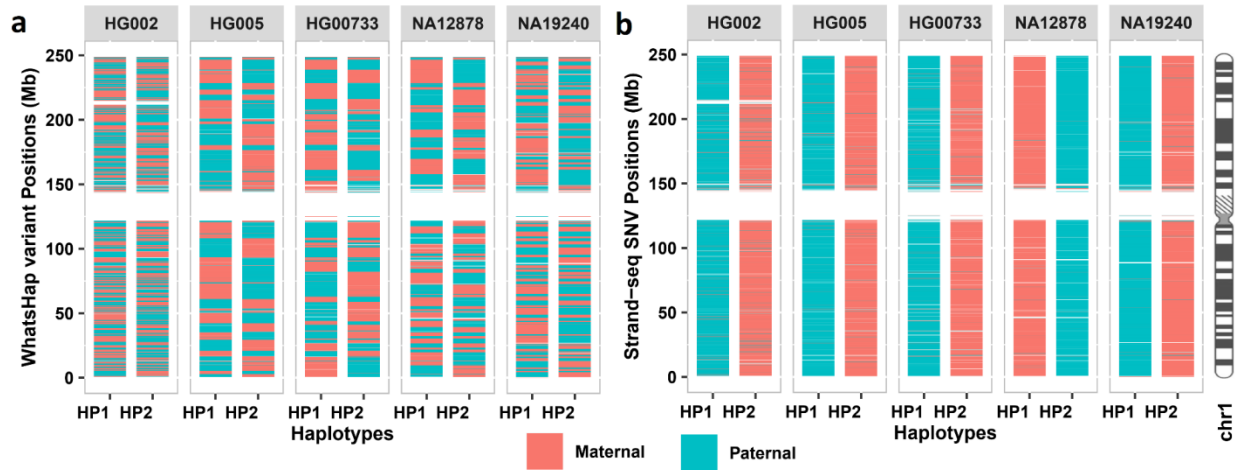


Libraries	66	42	182	64	220
Total unique reads ($\times 10^6$)	115	151	101	389	182
Total depth of coverage	2.78X	3.66X	2.96X	9.46X	5.81X

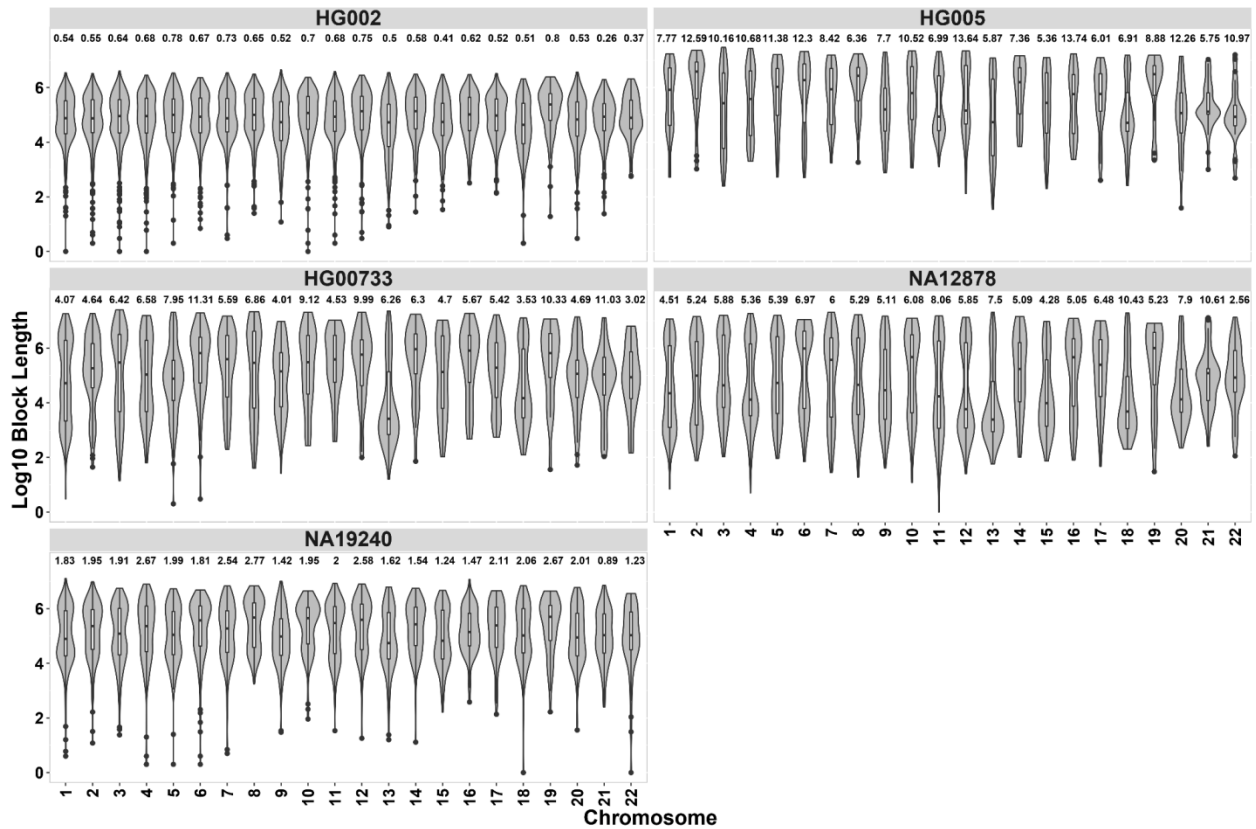
Supplementary Figure S2. Description of the Strand-seq libraries that passed QC and were used for phasing. Unique reads are mapped, non-duplicate reads with mapping quality at least 10. Related to the Results “Nanopore and Strand-seq enable chromosome-scale haplotyping” section and STAR Methods “Strand-seq phasing and inversion correction” section.



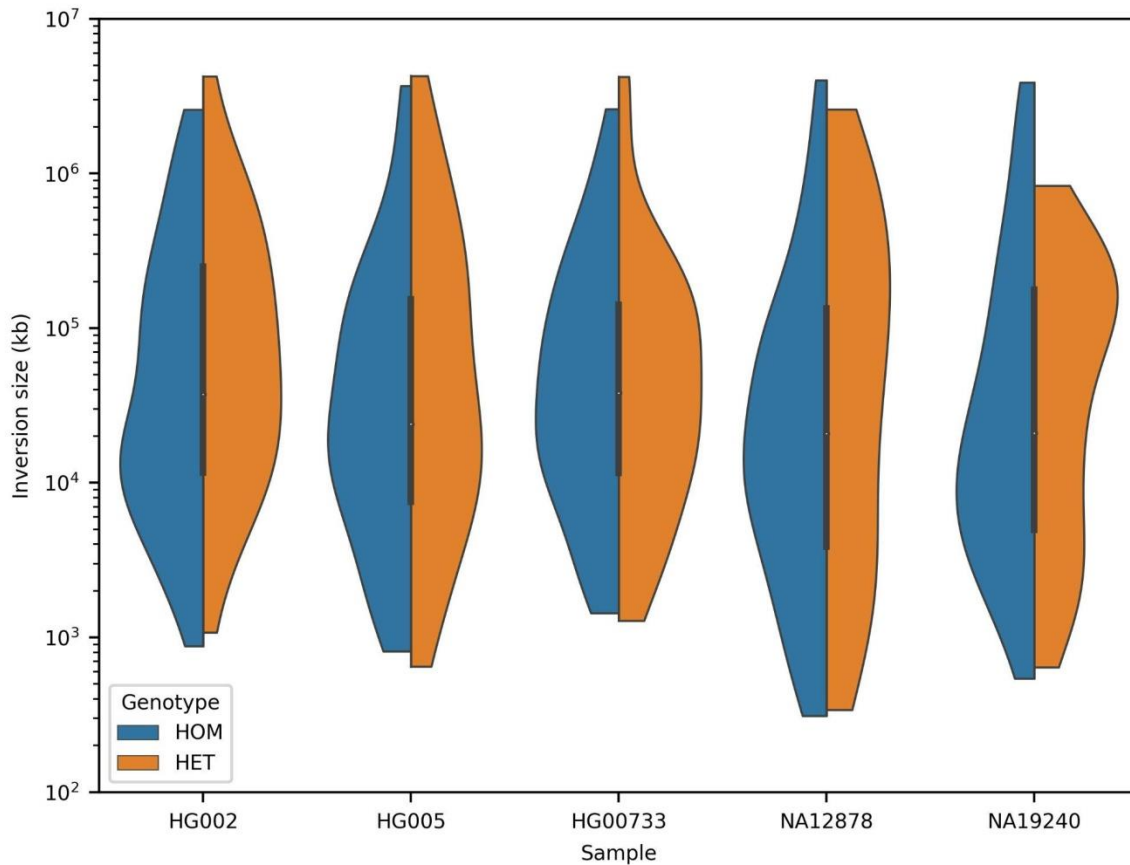
Supplementary Figure S3: Clair3 variant calling performance from nanopore data for HG002, HG005 and NA12878 cell lines. Ground truth high confidence variant calls and regions for these cell lines were obtained from GIAB (v4.2.1_benchmark). Nanopore-detected variants were then benchmarked against GIAB ground truth call sets and high confidence regions using hap.py (<https://github.com/Illumina/hap.py>). Because high confidence regions for HG00733 and NA19240 are not available, we did not benchmark these samples. Related to the Results “Nanopore and Strand-seq enable chromosome-scale haplotyping” section and STAR Methods “Nanopore data analysis” section.



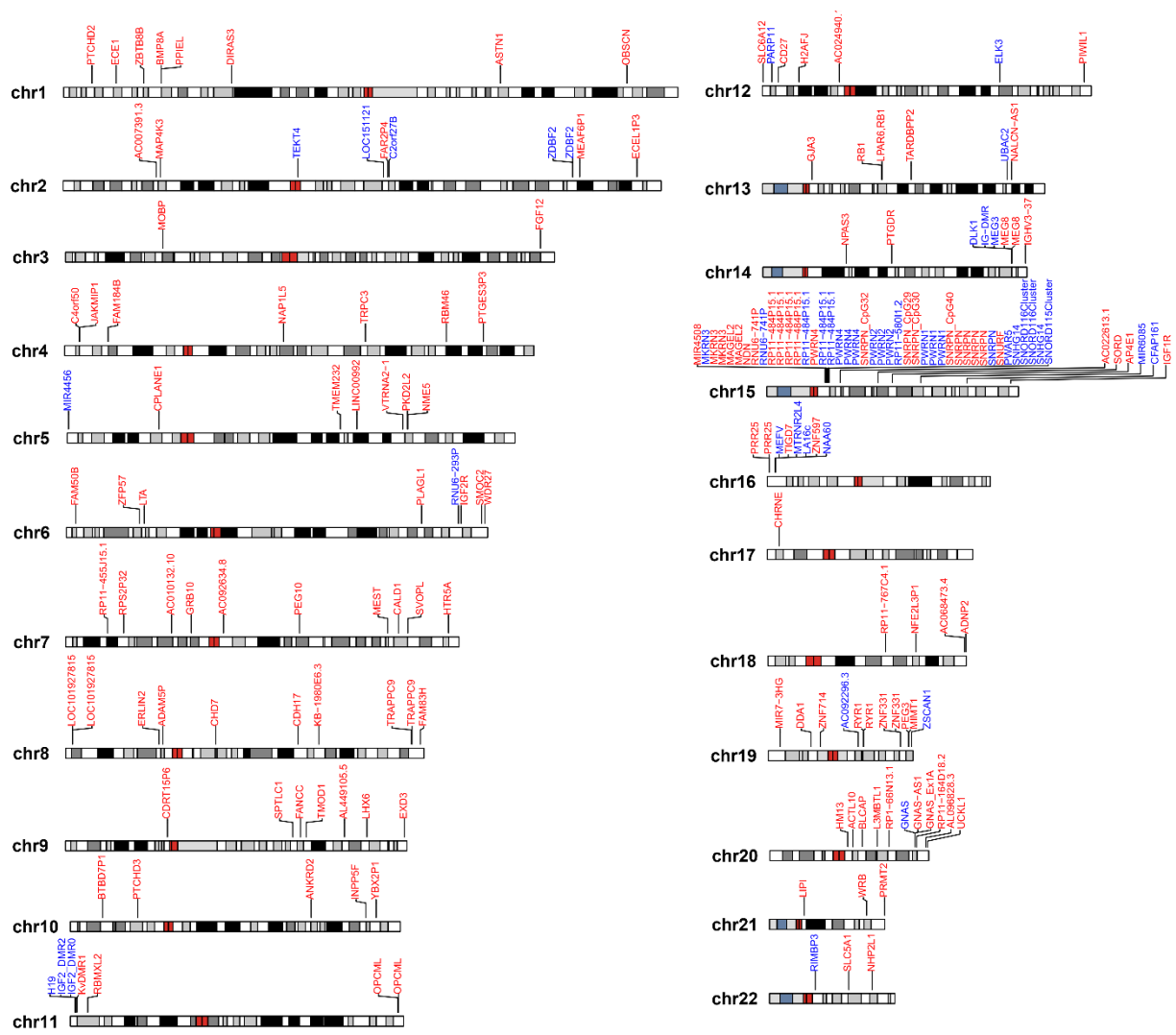
Supplementary Figure S4. Comparison of nanopore-only phasing and Strand-seq phasing. a) Subchromosomal nanopore phase blocks on chromosome 1 contain >99% of called SNVs and >96% of called indels. However, using nanopore-only phasing for PofO assignment results in per-chromosome $M \pm SD = 42.37\% \pm 7.13\%$ PofO errors of SNVs and $M \pm SD = 42.82\% \pm 6.83\%$ of indels (Supplementary Table S1). This is because arbitrary phase switches between phase blocks mean that PofO is effectively assigned at random for any phase block. WhatsHap v1.2.1 with the options `--indels --ignore-read-groups` was used to phase both indels and SNVs. b) By contrast, phasing nanopore-detected variants using Strand-seq results in chromosome-scale haplotypes with consistent PofO across each haplotype as shown here for chromosome 1 (Supplementary Table S1). Related to the Results “Nanopore and Strand-seq enable chromosome-scale haplotyping” section and STAR Methods “Nanopore data analysis” section.



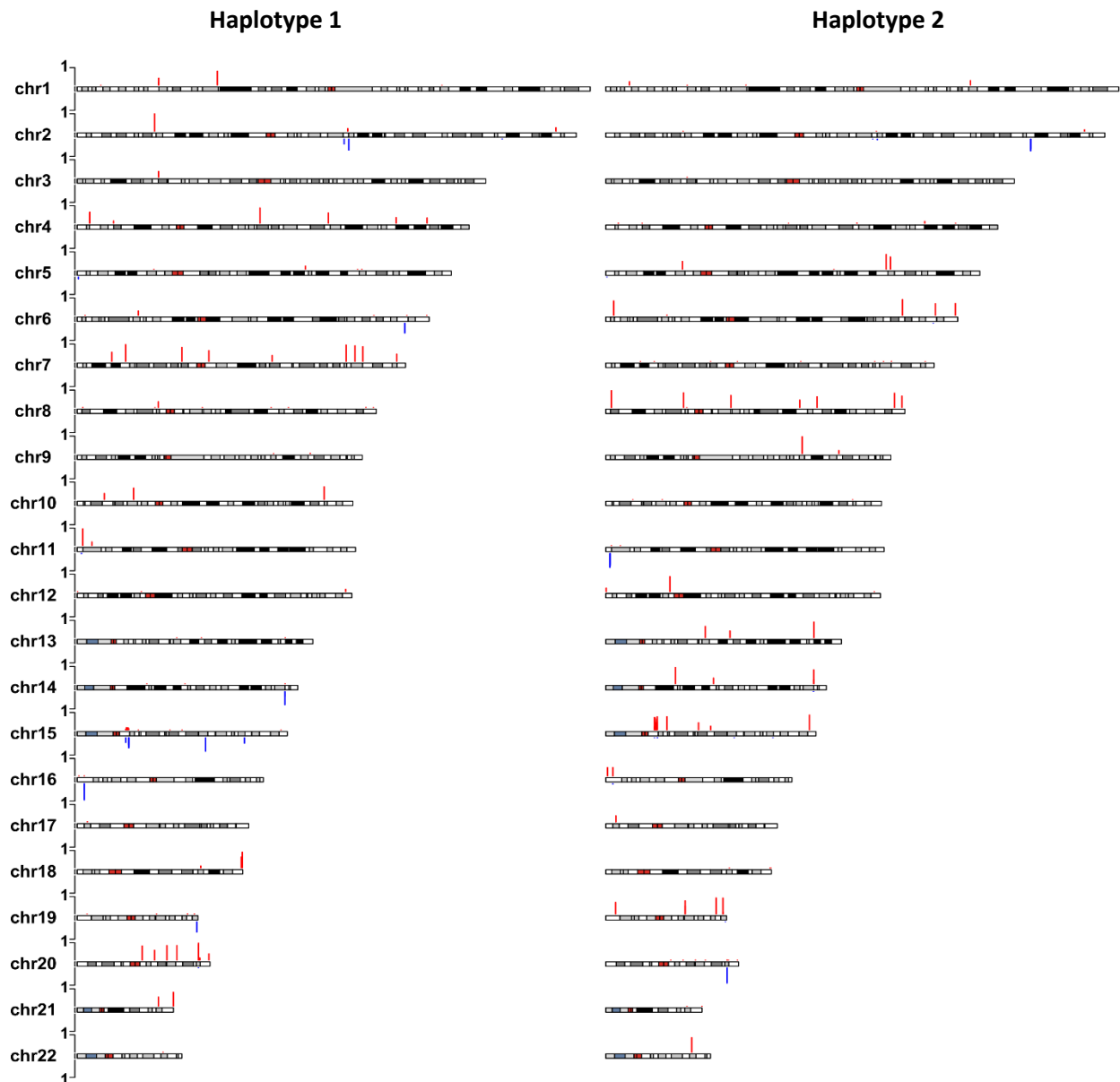
Supplementary Figure S5: Phase block sizes for phasing nanopore reads and heterozygous variants using WhatsHap (see Supplementary Figure 4). The numbers on top of the violins are N50 (Mb) that represents the shortest block size at which 50% of the length of the known human genome, GRCh38, is covered. Related to the Results “Nanopore and Strand-seq enable chromosome-scale haplotyping” section and STAR Methods “Nanopore data analysis” section.



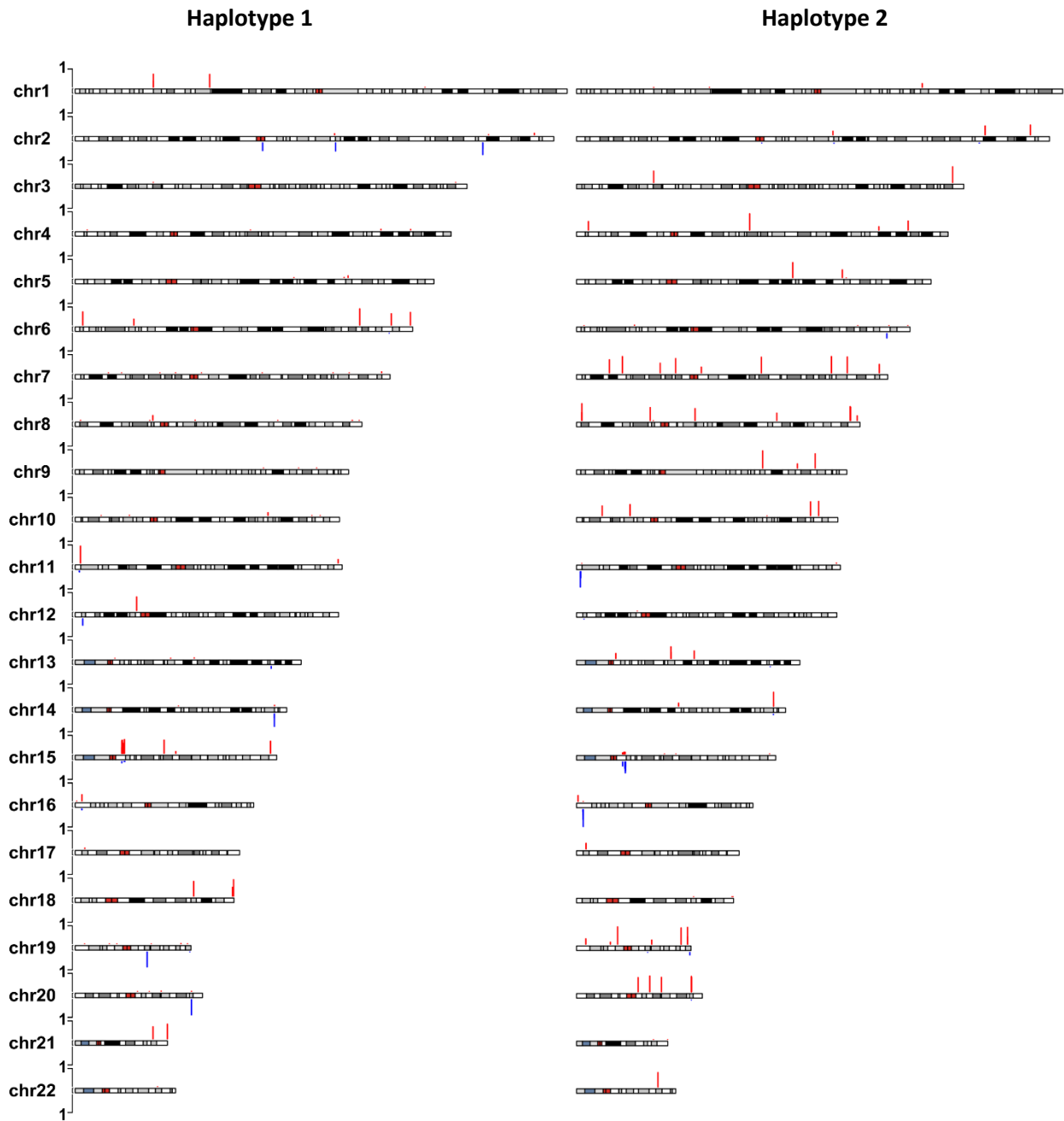
Supplementary Figure S6. Size distributions for the inversions identified with InverttypeR. Inversions smaller than 10 kb were not used for inversion-aware phasing. 29 inversions flagged as having low read density by InverttypeR, which indicates that they span regions of unmapped reads such as centromeres and have unreliable coordinates, were not included in this plot (out of 596 total inversions). In future, it may be possible to skip the inversion calling step and instead use a list of the locations of common polymorphic inversions to adjust variant phasing. Related to the Results “Nanopore and Strand-seq enable chromosome-scale haplotyping” section and STAR Methods “Strand-seq phasing and inversion correction” section.



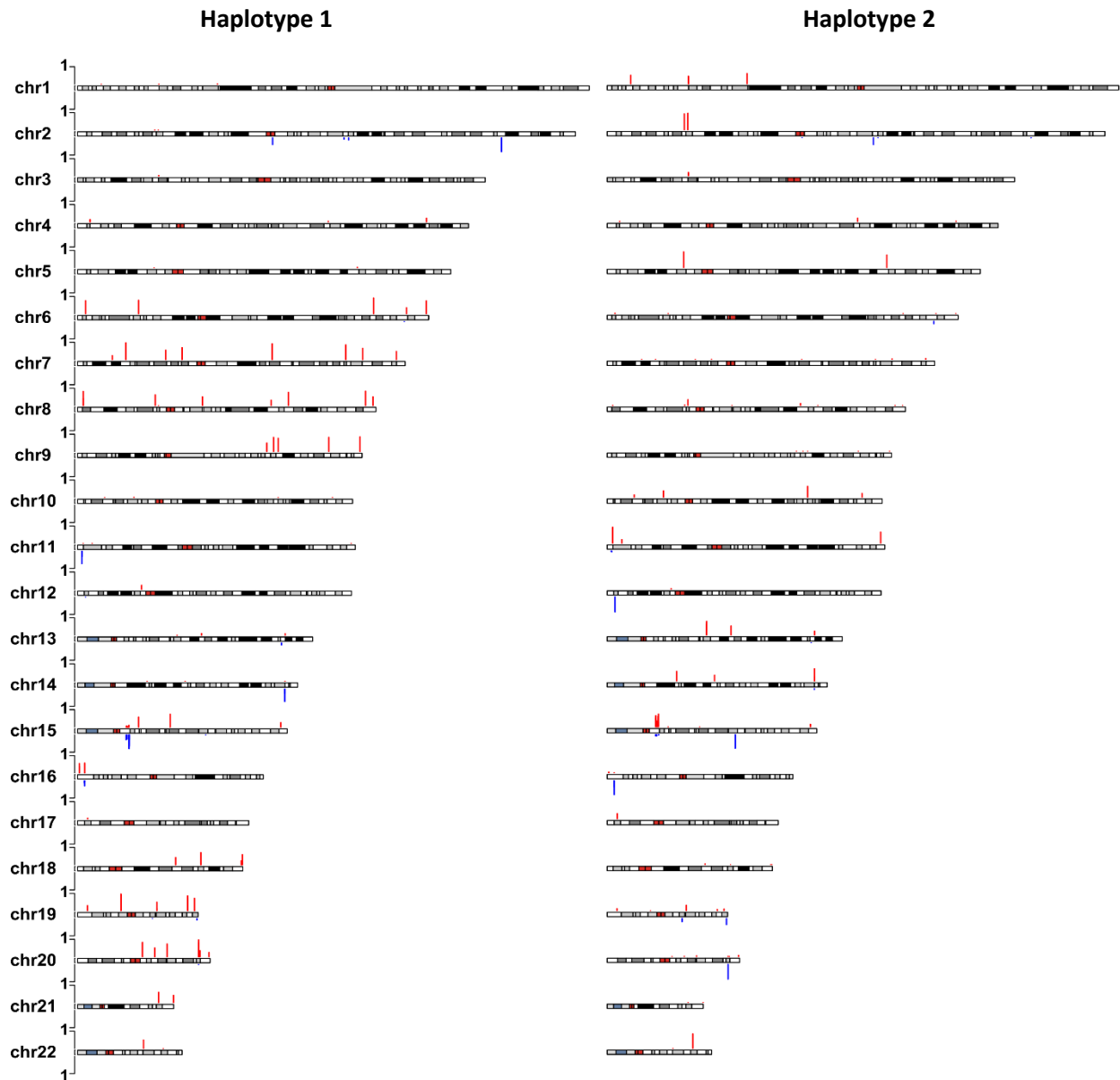
Supplementary Figure S7: Chromosome ideograms showing the selected iDMRs across the genome. Red represents maternally methylated iDMRs and blue paternally methylated iDMRs. Related to the Results “iDMRs assign PofO to haplotypes” section and STAR Methods “iDMR selection” section.



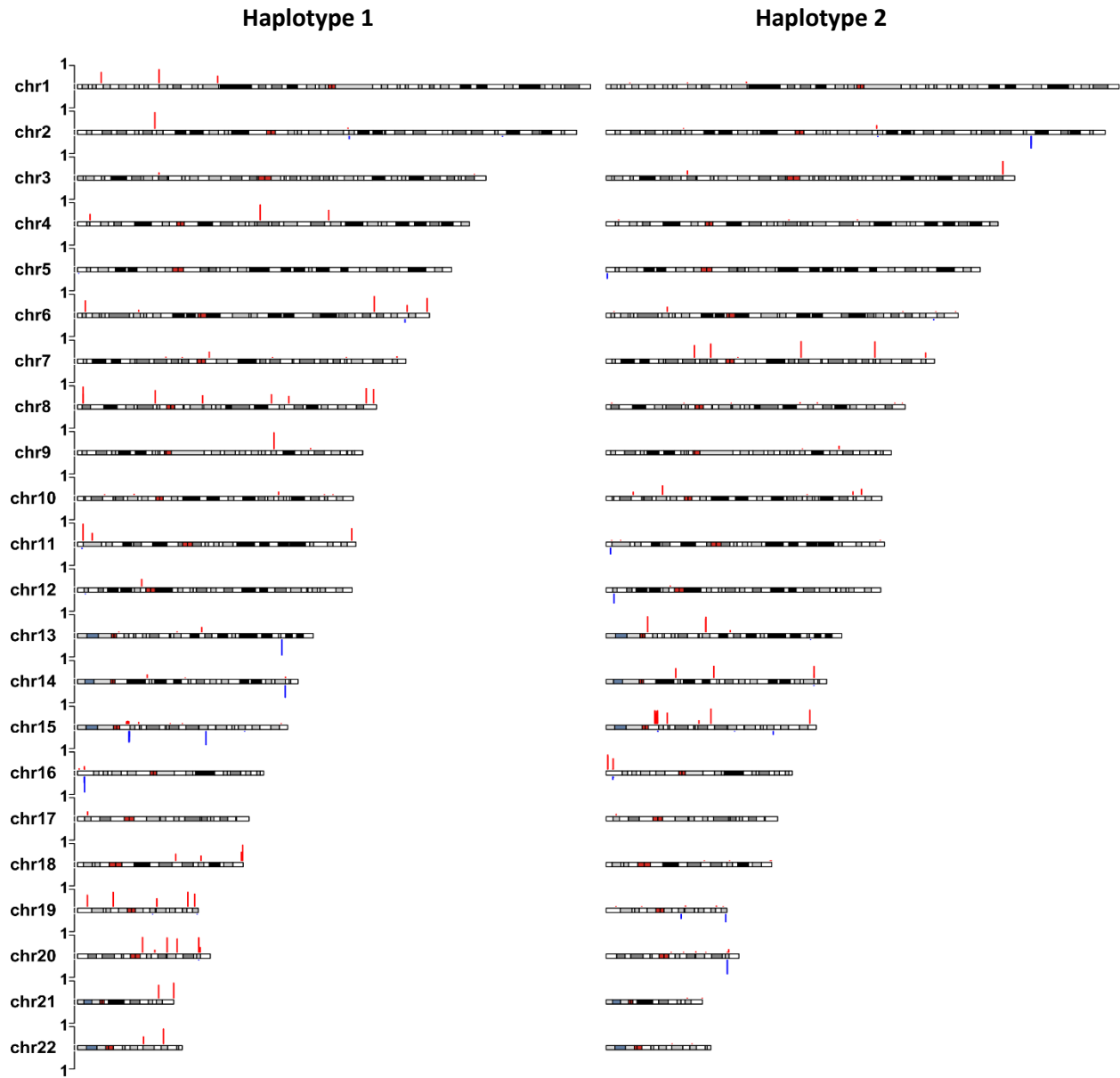
Supplementary Figure S8. CpG methylation at paternal and maternal iDMRs used for parent of origin assignment in HG005. Maternally methylated iDMRs are red and upward and paternally methylated iDMRs are blue and downward. Bars represent fraction of CpGs with methylation difference ≥ 0.35 between haplotypes (HP1 - HP2 for haplotype 1 and HP2 - HP1 for haplotype 2) at each iDMR for each haplotype. Related to the Figure 2.



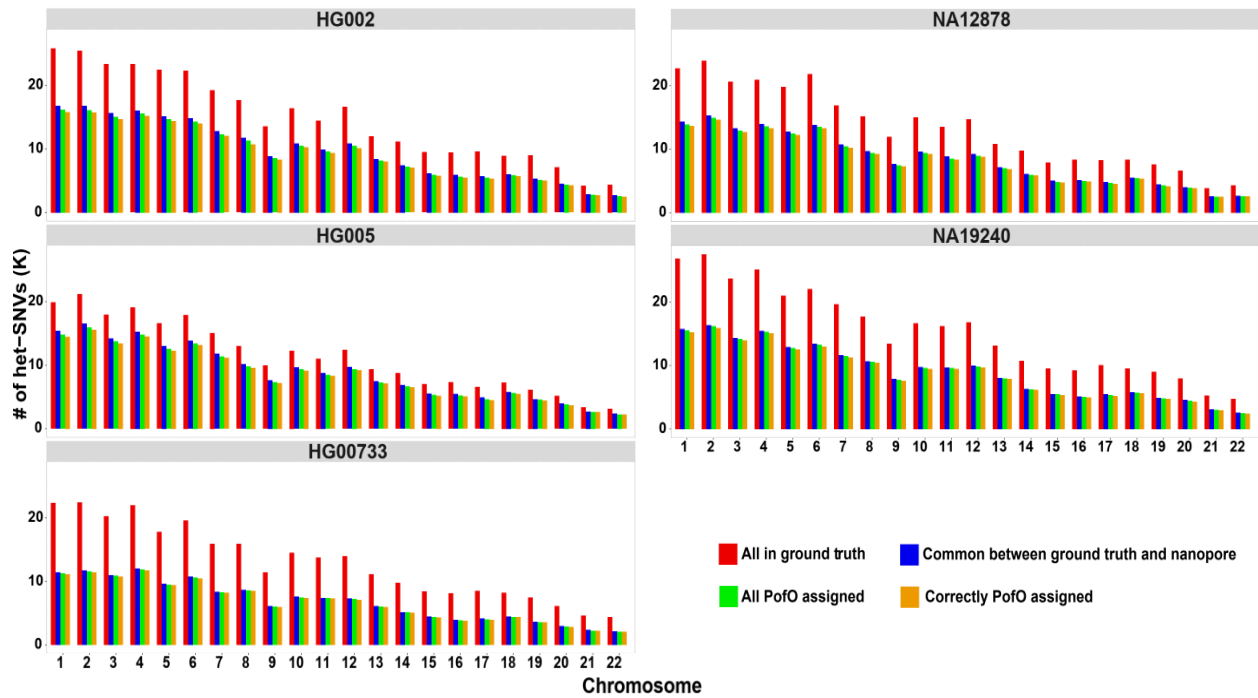
Supplementary Figure S9. CpG methylation at paternal and maternal iDMRs used for parent of origin assignment in HG00733. Maternally methylated iDMRs are red and upward and paternally methylated iDMRs are blue and downward. Bars represent fraction of CpGs with methylation difference ≥ 0.35 between haplotypes (HP1 - HP2 for haplotype 1 and HP2 - HP1 for haplotype 2) at each iDMR for each haplotype. Related to the Figure 2.



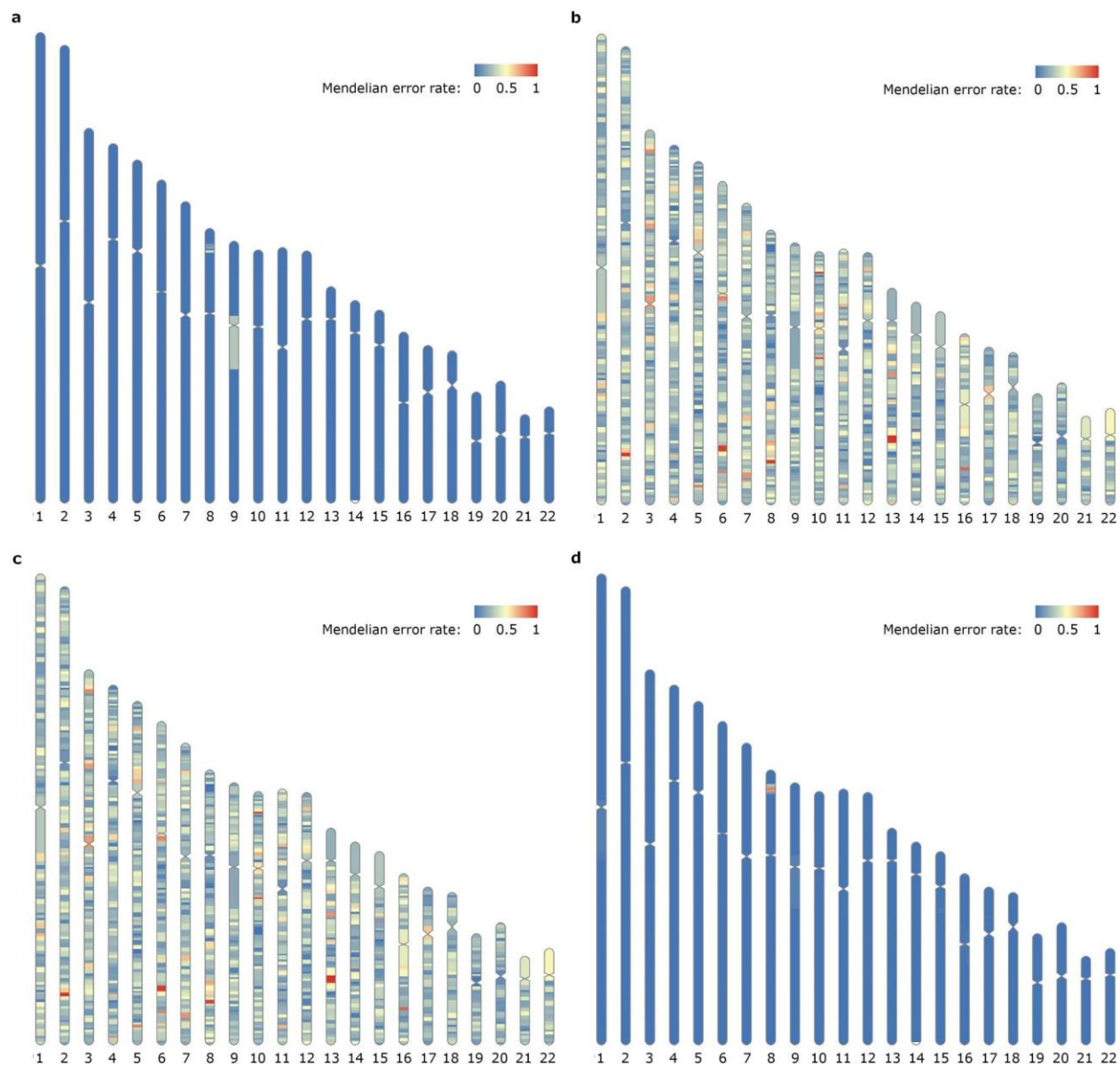
Supplementary Figure S10. CpG methylation at paternal and maternal iDMRs used for parent of origin assignment in NA12878. Maternally methylated iDMRs are red and upward and paternally methylated iDMRs are blue and downward. Bars represent fraction of CpGs with methylation difference ≥ 0.35 between haplotypes (HP1 - HP2 for haplotype 1 and HP2 - HP1 for haplotype 2) at each iDMR for each haplotype. Related to the Figure 2.



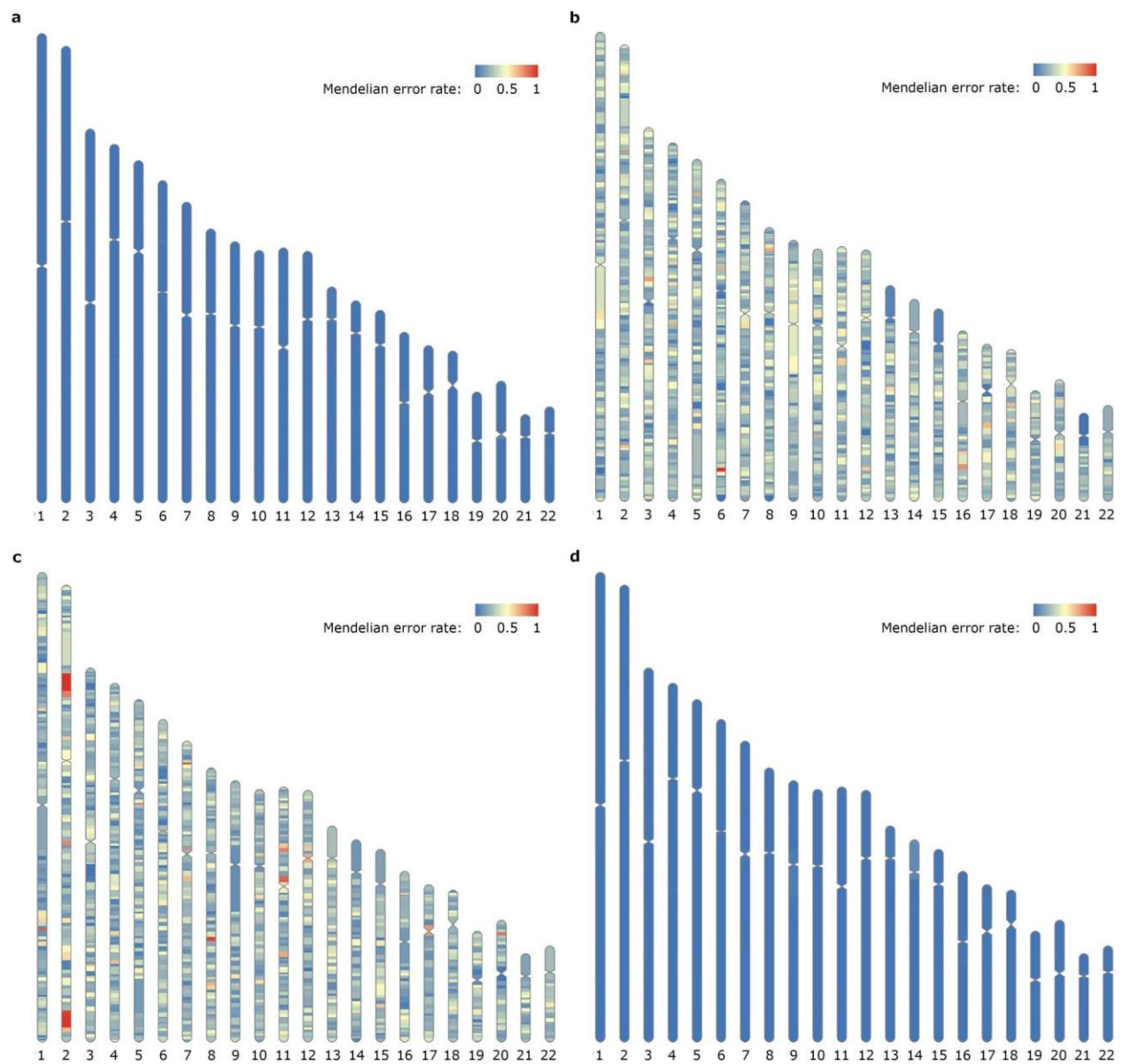
Supplementary Figure S11. CpG methylation at paternal and maternal iDMRs used for parent of origin assignment in NA19240. Maternally methylated iDMRs are red and upward and paternally methylated iDMRs are blue and downward. Bars represent fraction of CpGs with methylation difference ≥ 0.35 between haplotypes (HP1 - HP2 for haplotype 1 and HP2 - HP1 for haplotype 2) at each iDMR for each haplotype. Related to the Figure 2.



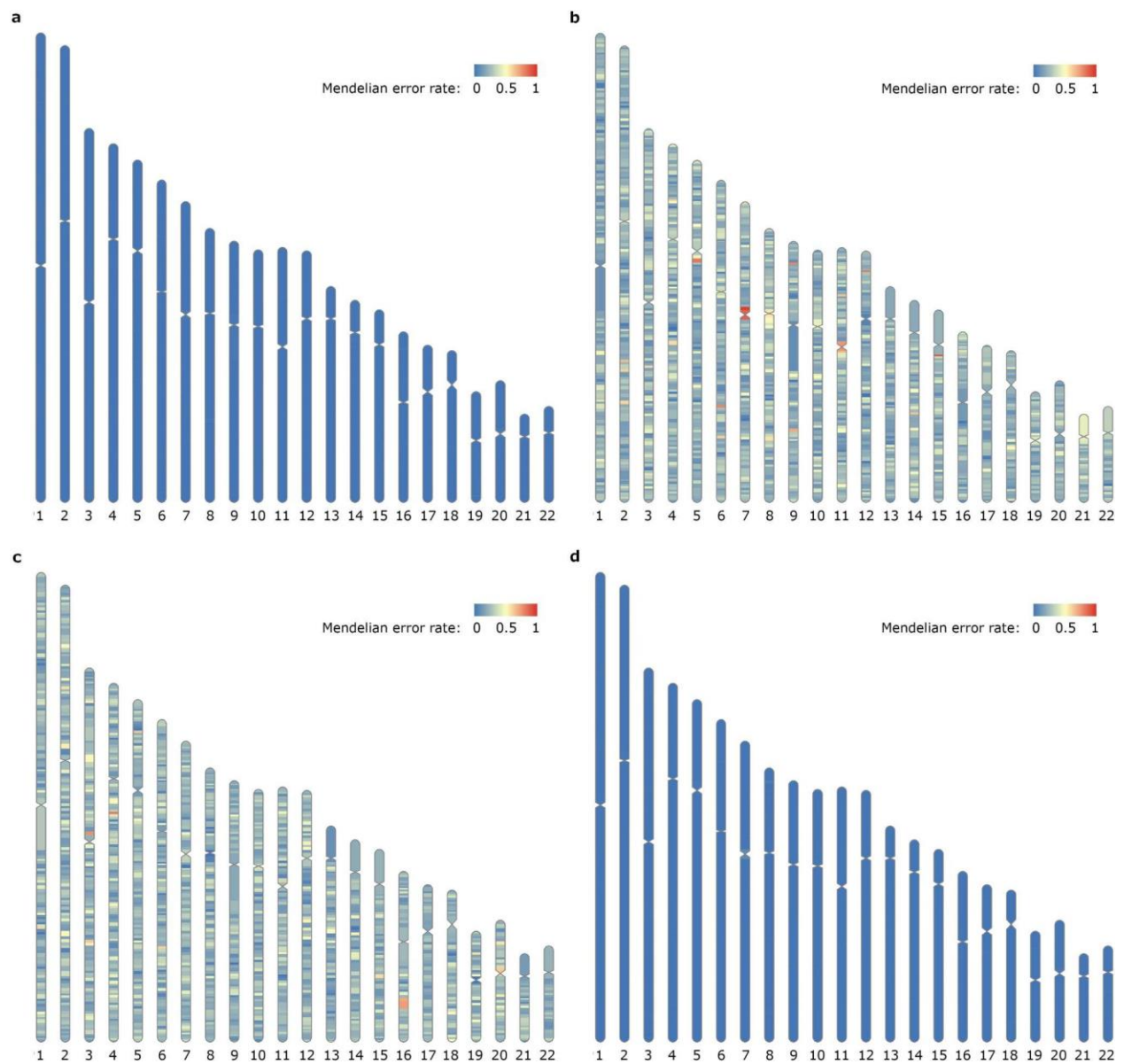
Supplementary Figure S12: Per-chromosome results for PofO assignment of het-Indels. PofO could be assigned to all homologs. The small fraction of variants with incorrect PofO are sporadic phasing errors in the Strand-seq or nanopore data. Related to the Figure 3.



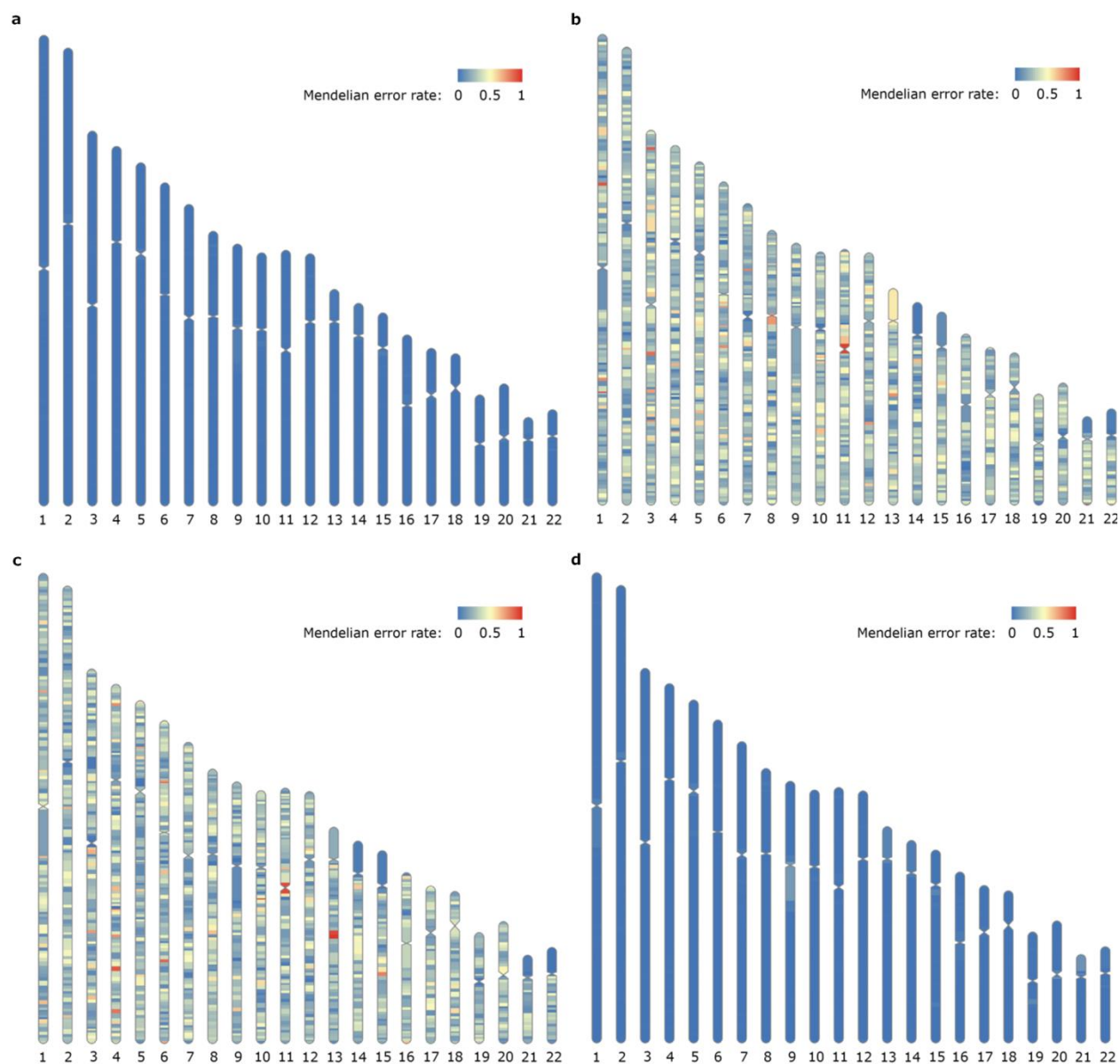
Supplementary Figure S13. Mendelian error rates for HG002. a) HG002’s inferred maternal haplotype compared with HG004 (mother). b) HG002’s inferred maternal haplotype compared with HG003 (father). c) HG002’s inferred paternal haplotype compared with HG004 (mother). d) HG002’s inferred paternal haplotype compared with HG003 (father). Regions of elevated Mendelian error rates are visible in a) and d) at the centromere for chromosome 9 (in a single bin of 1000 variants) and at a large common inversion on chromosome 8 (where the Strand-seq data and phasing software did not correctly account for the change to the aligned orientation of sequence reads inside the inversion). Related to the Figure 4.



Supplementary Figure S14. Mendelian error rates for HG00733. a) HG00733's inferred maternal haplotype compared with HG00732 (mother). b) HG00733's inferred maternal haplotype compared with HG00731 (father). c) HG00733's inferred paternal haplotype compared with HG00732 (mother). d) HG00733's inferred paternal haplotype compared with HG00731 (father). Related to the Figure 4.



Supplementary Figure S15. Mendelian error rates for NA19240. a) NA19240's inferred maternal haplotype compared with NA19238 (mother). b) NA19240's inferred maternal haplotype compared with NA19239 (father). c) NA19240's inferred paternal haplotype compared with NA19238 (mother). d) NA19240's inferred paternal haplotype compared with NA19239 (father). Related to the Figure 4.



Supplementary Figure S16. Mendelian error rates for NA12878. a) NA12878’s inferred maternal haplotype compared with NA12892 (mother). b) NA12878’s inferred maternal haplotype compared with NA12891 (father). c) NA12878’s inferred paternal haplotype compared with NA12892 (mother). d) NA12878’s inferred paternal haplotype compared with NA12891 (father). Related to the Figure 4.